AWARD NUMBER: DoD Award W81XWH-14-1-0086

TITLE: Targeting the S1P Axis and Development of a Novel Therapy for Obesity-Related Triple-Negative Breast Cancer

PRINCIPAL INVESTIGATOR: Sarah Spiegel

CONTRACTING ORGANIZATION: Virginia Commonwealth University
Richmond, VA 23298-0568

REPORT DATE: September 2017

TYPE OF REPORT: Annual

PREPARED FOR: U.S. Army Medical Research and Materiel Command
Fort Detrick, Maryland 21702-5012

REPORT DOCUMENTATION PAGE

Form Approved
OMB No. 0704-0188

1. REPORT DATE	2. REPORT TYPE	3. DATES COVERED
September 2017	Annual	1Sep2016 - 31Aug2017

4. TITLE AND SUBTITLE
Targeting the S1P Axis and Development of a Novel Therapy for Obesity-Related Triple-Negative Breast Cancer

5a. CONTRACT NUMBER

5b. GRANT NUMBER
W81XWH-14-1-0086

5c. PROGRAM ELEMENT NUMBER

6. AUTHOR(S)
Sarah Spiegel

Email: sarah.spiegel@vcuhealth.org

5d. PROJECT NUMBER

5e. TASK NUMBER

5f. WORK UNIT NUMBER

7. PERFORMING ORGANIZATION NAME(S) AND ADDRESS(ES)

Virginia Commonwealth University School of Medicine
Richmond, VA 23284

8. PERFORMING ORGANIZATION REPORT NUMBER

9. SPONSORING / MONITORING AGENCY NAME(S) AND ADDRESS(ES)
U.S. Army Medical Research and Materiel Command
Fort Detrick, Maryland 21702-5012

10. SPONSOR/MONITOR'S ACRONYM(S)

11. SPONSOR/MONITOR'S REPORT NUMBER(S)

12. DISTRIBUTION / AVAILABILITY STATEMENT
Approved for Public Release; Distribution Unlimited

13. SUPPLEMENTARY NOTES

14. ABSTRACT

The majority of breast tumors express the estrogen receptor α (ERα), which plays important roles in breast cancer pathogenesis and progression, and hormonal therapies, such as tamoxifen, are the first line of adjuvant therapy (1, 2). Unfortunately, half of these patients will ultimately fail therapy due to de novo or acquired resistance. Moreover, patients with ER, progesterone receptor (PR) and human epidermal growth factor receptor 2 (HER2, also known as ErbB-2) triple negative breast cancer (TNBC), which is aggressive with high recurrence, metastatic, and mortality rates (3), do not respond to hormonal therapies and have limited treatment options. Epidemiological and clinical studies indicate that obesity, which is now endemic, increases breast cancer risk and is associated with worse prognosis (4), which may be due in part to the high frequency of TNBC and ineffectual hormonal therapy (5). However, the links between obesity and breast cancer are not understood and is the focuse of our study. As hormonal therapy is so effective with relatively few side effects, the possibility of reversing hormonal unresponsiveness is an appealing treatment approach. Our study will lead to novel therapies that will overcome the overarching challenges of developing safe and effective drugs for treating obesity-promoted cancers and TNBC and will identify the bioactive sphingolipid metabolite, sphingosine-1-phosphate (S1P), produced by sphingosine kinases (SphK1 and SphK2), as a critical factor that links obesity and chronic inflammation to drive breast cancer growth and metastasis.

15. SUBJECT TERMS-

Nothing listed

16. SECURITY CLASSIFICATION OF:			17. LIMITATION OF ABSTRACT	18. NUMBER OF PAGES	19a. NAME OF RESPONSIBLE PERSON
a. REPORT	b. ABSTRACT	c. THIS PAGE			USAMRMC
U	U	U	UU	54	19b. TELEPHONE NUMBER *(include area code)*

Table of Contents

Page

1. INTRODUCTION

Breast cancer affects nearly 1 out of every 8 women over their lifetime and is the second leading cancer cause of death for women behind lung cancer in the US. Fortunately, over the last 30 years, breast cancer death rates have been dropping due to increased awareness of the disease, advances in detection, and better treatments. A large factor in these better treatments has been development of hormonal therapies to directly target specific receptors in the cancer cells such as estrogen (ER) and progesterone receptors (PR) that are present in roughly 70% of breast cancers. ER positive tumors in particular can be treated with estrogen antagonists such as tamoxifen to great effect with less side effects than traditional chemotherapy. The human epidermal growth factor receptor 2 (HER2), that is upregulated in 10 to 15% of breast cancers tumors can also be treated with a monoclonal antibody. However, there are still 15 to 20% of tumors that are ER/PR/HER2 negative, termed triple negative breast cancer (TNBC), which are usually more aggressive and metastatic with significantly worse prognosis. Therefore, current cancer research is also focused on deeper understanding of novel signaling pathways that can contribute to breast cancer growth and metastasis. Our work demonstrates that the bioactive sphingolipid metabolite, sphingosine-1-phosphate (S1P), regulates processes important for breast cancer including inflammation that can drive tumorigenesis, angiogenesis, which provides cancer cells with nutrients and oxygen, cell growth and survival, as well as migration and invasion important for metastasis (Maczis et al., 2016). In particular, one of the kinases that produces S1P, sphingosine kinase 1 (SphK1), is commonly upregulated in breast cancer cells and has been linked with poorer prognosis and progression, possibly leading to resistance to certain anti-cancer therapies (Datta et al., 2014; Gao et al., 2015; Ruckhaberle et al., 2008). Recently, our lab discovered that the other isoform, SphK2, also plays an important role in breast cancer progression and metastasis. We also recently discovered an unrecognized function of Spns2, a specific S1P transporter, in pulmonary metastatic colonization. We hope that our study will lead to novel therapies that will overcome the overarching challenges of developing safe and effective drugs for treating obesity-promoted cancers, metastatic breast cancer, and TNBC and will identify the bioactive sphingolipid metabolite, S1P produced by SphK1 and SphK2, as a critical factor that drives breast cancer growth and metastasis.

2. KEY WORDS

sphingosine-1-phosphate, sphingosine kinase, FTY720 (fingolimod, Gilenya), triple negative breast cancer, ERα, obesity, histone deacetylase, inflammation, tamoxifen resistance

3. ACCOMPLISHMENTS

3.1. Major Goals of the Project

Our project has three major aims.

Aim 1. Determine the role of SphK1 and S1P in obesity promoted chronic inflammation and tumor progression and decipher the molecular links between the SphK1-S1P-S1PR1 axis and persistent NF-kB and STAT3 activation.

Aim 2. Target the SphKs/S1P/S1PR1 axis with fingolimod/FTY720 for treatment of obesity associated breast cancer to suppress the malicious amplification cascade, and reactivate ER expression in ER-negative breast cancer.

Aim 3. Examine the association of the SphKs/S1P/S1PR1 axis in human breast cancer and prognosis.

The inability to effectively predict, prevent, and treat metastatic breast cancer is a major problem in breast cancer care. This proposal provides evidence that the SphKs/S1P/S1PR1 axis is one of the critical factors that drive breast cancer growth and metastasis and paves the way for development of new adjuvant therapies targeting this axis as a promising strategy for effective treatment of advanced and refractory breast cancer.

3.2. Accomplishments Under These Goals and Significant Results

Targeting the SphK1/S1P/S1PR1 axis that connects obesity, chronic inflammation, and breast cancer metastasis.

Obesity with associated inflammation is now recognized as a risk factor for breast cancer and increased incidence of distant metastases (Neuhouser et al., 2015). However, the link between obesity and breast cancer remains poorly understood. In a recent study that has been submitted to Cancer Research, we demonstrated that obesity increases levels of the bioactive sphingolipid mediator S1P in breast cancer patients and in animal breast cancer models that we previously described (Hait et al., 2015). High fat diet also upregulated expression of SphK1, the enzyme that produces S1P, and its receptor S1PR1 in syngeneic and spontaneous breast tumors. Targeting the SphK1/S1P/S1PR1 axis with FTY720/fingolimod attenuated obesity-induced key pro-inflammatory cytokines, macrophage infiltration, and tumor progression. Furthermore, S1P produced by tumor SphK1 primed lung pre-metastatic niches, increased macrophage recruitment into the lung, and induced the pro-inflammatory cytokine IL-6 and signaling pathways important for lung metastatic colonization. FTY720 suppressed high fat diet induced lung IL-6 and macrophage infiltration as well as S1P-mediated signaling pathways and dramatically reduced formation of metastatic foci. In tumor bearing mice, FTY720 also reduced obesity-related inflammation, S1P signaling, pulmonary metastasis, and prolonged survival (Nagahashi et al, 2017). We believe that our results highlight a critical role for circulating S1P produced by tumor and the SphK1/S1P/S1PR1 axis in obesity-related inflammation, metastatic niche formation and breast cancer metastasis and suggest that targeting the SphK1/S1P/S1PR1 axis may be a useful therapeutic for obesity promoted metastatic breast cancer.

Genome-wide screen identifies the S1P transporter Spns2 as a novel host regulator of pulmonary metastatic colonization in breast cancer

Metastasis is the leading cause of death for breast cancer patients. This multi-stage process requires tumor cells to survive in the circulation, extravasate at distant sites, then proliferate; it involves contributions from both the tumor cell and tumor microenvironment that includes stromal cells and the immune system. It is well established that the early steps of the metastatic process are relatively efficient, with the post-extravasation regulation of tumor growth ('colonization') being critical in determining metastatic outcome. Our collaborators at the UK Sanger Institute screened 810 mutant mouse lines using an in vivo assay of tail vein injections of B16 melanoma cells to identify microenvironmental regulators of metastatic colonization. Intriguingly, they found that the largest reduction in pulmonary metastasis was observed in S1P transporter Spns2 knockout mice (van der Weyden et al., 2017). Together, we also found that Spns2 deletion in lymphatic endothelial cells also decreased pulmonary metastatic colonization of E0771.LMB cells, an aggressive murine breast cancer cell line (Fig. 1A).

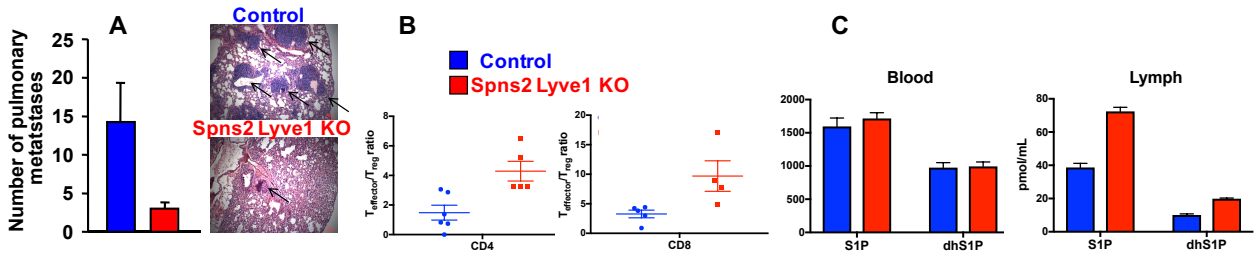

Figure 1. Lymphatic endothelial cell specific deletion of Spns2 increases effector T cells in the lung and decreases pulmonary metastatic colonization. Wild type and lymphatic endothelial cell specific deletion of Spns2 (Spns2 Lyve1 KO) mice were injected intravenously with E0771.LMB cells. After 35 d, lungs were removed. (A) Lung nodules were counted and lung sections were stained with H&E. Arrows indicate lnodules. (B) Lung effector and regulatory T-cells were analyzed by flow cytometry.

(C) Levels of S1P and dihydro-S1P (dhS1P) in blood and lymph were determined by LC-ESI-MS/MS.

Furthermore, similar to Spns2 globally deleted mice, we found that there was a higher percentage of anti-tumoral effector memory T cells ($CD44^{hi}CD62L^{lo}$) compared to immune suppressive regulatory T cells ($CD4^{+}CD25^{+}$), leading to an increased effector:regulatory T cell ratio in the lung of lymphendothelial specific Spns2 deleted mice (Fig. 1B). We suggest that this allows for potent tumor cell killing and decreased metastatic burden. Surprisingly, although blood levels of S1P were not altered, we observed that levels of S1P and dihydro-S1P were increased in lymph concomitant with decreased metastatic colonization (Fig 1C). Further studies are underway to understand how Spns2 controls levels of S1P in the circulation and particularly in lymph to regulate the S1P gradient, lymphocyte trafficking, and consequently affect breast cancer cell killing.

Metastasis of breast tumors is greatly decreased by deletion or inhibition of SphK2

We recently published that SphK2 knockout mice similar to Spns2 lymphendothelial specific deleted mice also have increased lymph S1P (Nagahashi et al., 2016). Therefore, we next examined the role of SphK2 in pulmonary metastatic colonization. Remarkably, we found that breast tumor growth and lung metastasis were greatly suppressed in female SphK2 knockout mice compared to littermate controls (Fig. 2A). Moreover, SphK2 deletion greatly reduced tumor infiltrating immunosuppressive cells, including myeloid derived suppressor cells (MDSCs) and T-regs, and greatly increased CD4 and CD8 effector T cells (Fig. 2A and data not shown). In addition, pulmonary metastatic colonization was greatly reduced when wild type mice were treated the SphK2 inhibitor SLM6013434 (Kharel et al., 2015) (Fig. 2B). Once again, inhibition of SphK2 greatly reduced MDSCs and T-regs in the lung and increased CD4 and CD8 effector T cells. This is the first demonstration of the critical role of SphK2 in regulation of breast cancer metastasis. As metastasis is the leading cause of death of breast cancer patients, our work suggests that targeting SphK2, Spns2 and the S1P gradient are potentially promising options for suppressing breast cancer metastasis.

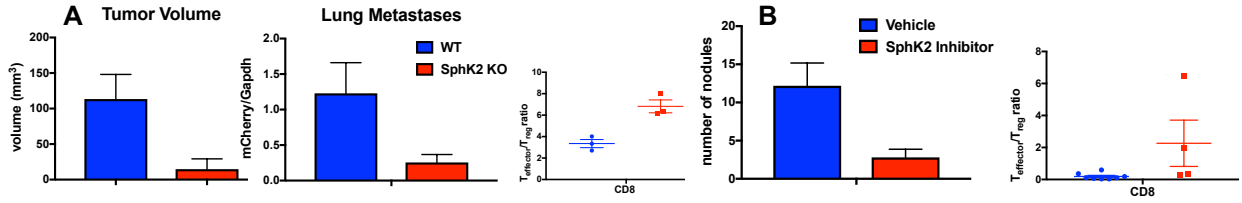

Figure 2. Growth and metastasis of syngeneic breast tumors is decreased by SphK2 deletion or inhibition. (A) Murine E0771.LMB breast cancer cells were implanted in the mammary fat pads of wild type and SphK2 knockout female mice. Mice were sacrificed 35 d later and tumor volume measured. Metastasis to the lungs was assessed by mCherry mRNA normalized to Gapdh. Tumor immune cell infiltrates were analyzed by flow cytometry. (B) C57Bl/6 wild-type male mice were intravenously injected with E0771.LMB cells and then treated with the SphK2 inhibitor SLM6013434 (2 mg/kg) or vehicle. After 35 d, lung nodules were counted and tumor immune cell infiltrates were analyzed by flow cytometry.

3.3. Opportunities for Training and Professional Development

Although the project was not designed to provide training and professional development opportunities, we should point out that the VCU School of Medicine developed several new programs for enhancing training and professional development of graduate students and postdoctoral fellows in recognition of the important roles they fulfill. This provides them with career and mentoring resources including FASEB Individual Development Plan, Individual Development Plan web-based tool, job opportunities in BioCareers, career resources from AAAS, CV/resume writing and samples from UCSF Office of Career and Professional Development, career development websites. For graduate students, these functions reside

within the Office of Graduate Education. While no graduate students were included in the original proposal, Melissa Maczis, who rotated in my lab during her first year as a PhD student, decided to join my lab two years ago and was supported by the VCU School of Medicine for the first two years. I have already begun advising her on career development. Using the "my Individual Development" plan website, she created an Individual Development Plan (IDP) she is using to record the immediate and long term objectives of her research and plan of her career path. She has been making outstanding progress toward accomplishing her career goals and received a F31 fellowship from NIH.

3.4. How were the results disseminated to communities of interest

We presented several research lectures on this project to the cancer research community at the Massey Cancer Center Retreat and in the regular meetings of the Massey Cancer Center Cancer Cell Signaling Program, which I direct together with Dr. Andrew Larner. We also presented this work to the international scientific community in several Keynote lectures (See below).

3.5 The Plan for the Next Reporting Period

Continue as was proposed in the original application. As mentioned above, we have already made substantial progress in Aim 1 and completed Aim 2 and have also continued to accomplish Aim 3. As discussed above, we have uncovered previously unknown important links between Spns2 and SphK2 to lung metastasis in breast cancer that we intend to pursue further.

4. IMPACT

4.1. The impact on the development of the principal discipline of the project

As mentioned in the previous report, our work suggests that a multi-pronged attack with FTY720 is a novel combination approach for effective treatment of conventional hormonal therapy-resistant breast cancer and triple-negative breast cancer. FTY720 has several advantages over available HDAC inhibitors as potential treatments for breast cancer patients: it is an orally bio-available pro-drug; it has already been approved for human use; it regulates expression of only a limited number of genes (a majority related to cholesterol and sphingolipid metabolism) compared to other HDAC inhibitors; it has good pharmacokinetics and a long half life; it suppresses several survival and proliferative pathways; and it is much less toxic, accumulates in tumor tissues, and both the phosphorylated and unphosphorylated forms target important pathways in breast cancer. Hence, we hope that our studies will pave the way for exploration of new clinical trials using FTY720 as a prototype of new adjuvant treatment strategies for hormonal resistant breast cancer. This might be particularly relevant in view of the increase in obesity that is now endemic and in de novo and acquired resistance to hormonal therapy. More recently, our work also suggests that targeting other components of the S1P axis such as the S1P transporter Spns2 and SphK2, might be especially beneficial for metastatic breast cancer.

4.2. The Impact on Other Disciplines

Although this work may not have a direct impact on other disciplines it might contribute to them, particularly in the treatment of cognitive impairment. HDAC inhibitors have shown promise as a treatment to combat the cognitive decline associated with aging and neurodegenerative disease, as well as to ameliorate the symptoms of depression and posttraumatic stress disorder, among others. Due to its unique features described above and its high brain penetration, FTY720 might be more effective than other HDAC inhibitors as an adjuvant therapy for erasing aversive memories (Hait et al., 2014). This might also be relevant to suppression of cognitive impairment and neuropathic pain associated with chemotherapy. Moreover, our recent

work shows that targeting the S1P/S1PR1 axis by treatment with FTY720 greatly reduces cancer-induced bone pain and neuroinflammation (Grenald et al., 2017) and supports potential fast-track clinical application of the FDA-approved drug, FTY720, as a therapeutic avenue for cancer-induced bone pain.

4.3. The Impact on Technology Transfer
Nothing to report
4.4. The impact on Society Beyond Science and Technology
Nothing to report

5. CHANGES/PROBLEMS

There are no significant changes in the project or its direction. We are pursuing our interesting results on the role of SphK2 in breast cancer growth and particularly in pulmonary metastasis. However, Melissa Maczis received her own fellowship from NIH (F31CA220798). Therefore, her salary will no longer be covered by the DOD. We are also in the process of interviewing other candidates to help finish this exciting work.

6. PRODUCTS

Publications

1. van der Weyden L, Arends MJ, Campbell AD, Bald T, Wardle-Jones H, Griggs N, Velasco-Herrera MD, Tüting T, Sansom OJ, Karp NA, Clare S, Gleeson D, Ryder E, Galli A, Tuck E, Cambridge EL, Voet T, Macaulay IC, Wong K; Sanger Mouse Genetics Project, **Spiegel S**, Speak AO, Adams DJ. Genome-wide in vivo screen identifies novel host regulators of metastatic colonization. Nature. 2017, Jan 12;541(7636):233-236. doi: 10.1038/nature20792.
2. Keffken K and **Spiegel S**. Sphingosine Kinase 1 in Breast Cancer. Adv. Biol. Regul. 2017, In Press
3. Nagahashi M, Yamada A, Aoyagi T, Huang W-C, Terracina KP, Hait NC, Allegood JC, Tsuchida J, Nakajima M, Katsuta E, Milstien S, Wakai T, **Spiegel S** and Takabe K. Targeting the SphK1/S1P/S1PR1 axis that connects obesity, chronic inflammation, and breast cancer metastasis. Cancer Res. 2017, In revision.

Abstracts

1. Sarah Spiegel, Sphingosine-1-phosphate: A Bridge from Bench to Clinic. ASBMB 2016 Annual Meeting, San Diego, CA. April 2-6, 2016 #243.1
2. Sarah Spiegel, Sphingosine-1-phosphate: From bench to translational Medicine. Lipid Mediators In Health and Disease II, La Jolla, CA. May 19-20, 2016
3. Sarah Spiegel, Sphingosine-1-phosphate at the cross roads between cancer and inflammation. FASEB Summer Research Conference, Phospholipid Signaling in Cancer, Neurodegeneration and Cardiovascular Disease, Steamboat Springs, CO. July 31-August 5, 2016
4. Sarah Spiegel and Melissa Maczis, Role of sphingosine-1-phosphate in estrogen receptor signaling in breast cancer, Rapid Response to Steroid Hormones Conference, VCU, Richmond, VA. November 2-5, 2016
5. Sarah Spiegel and Sheldon Milstien, Targeting the Sphingosine-1-Phosphate Axis and Development of a Novel Therapy for Endocrine-Resistant Breast Cancer, Keystone Symposium on Lipidomics and Bioactive Lipids in Metabolism and Disease, Lake Tahoe, CA, February 26-March 2, 2017
6. Sarah Spiegel, A Bridge from Bench to Clinic, Celgene, Boston, MA, February 3, 2017

7. Sarah Spiegel, Sphingosine-1-phosphate, from insipid lipid to key regulator of lymphocyte trafficking and the link between inflammation and cancer, UCSD, San Diego, CA, February 14, 2017
8. Sarah Spiegel and Sheldon Milstien, Role of Sphingosine-1-Phosphate in Estrogen Signaling in Breast Cancer, Keynote Lecture, 5th World Breast Cancer Conference, London, UK June 15-17, 2017
9. Sarah Spiegel and Sheldon Milstien, New Aspects of Sphingosine-1-Phosphate in Inflammation and Cancer, FASEB Research Conference on Lysophospholipid and Related Mediators – from Bench to Clinic, New Orleans, LA, August 20-25, 2017
10. Melissa Maczis, Sheldon Milstien, Sarah Spiegel, Role of Sphingosine-1-Phosphate in Non-Genomic Effects of Estradiol in Triple Negative Breast Cancer, FASEB Research Conference on Lysophospholipid and Related Mediators – from Bench to Clinic, New Orleans, LA, August 20-25, 2017
11. Sarah Spiegel, Keynote Lecture, New Aspects of Sphingosine-1-Phosphate in Cancer, XII Sphingolipid Club Meeting, Trabia, Sicily, Italy, September 6-10, 2017

7. PARTICIPANTS & OTHER COLLABORATING ORGANIZATIONS

Individuals that have worked on the project

Name: Sarah Spiegel
Project Role: PI – No change

Name: Sheldon Milstien
Project Role: Co-Investigator – No change

Name: Kazuaki Takabe
Project Role: Co-Investigator – Left VCU June 2016, now at Roswell Park, Clinical Chief of Breast Surgery and Breast Disease Site Leader. We will continue our long-standing collaboration but his salary is covered by his new institution.

Name: Melissa Maczis
Project Role: Graduate Student
Will continue to work on this project. However, since she is an outstanding student, she received a fellowship from NIH and her salary starting July 1, 2017 will not be covered by the current DOD grant.

Has there been a change in the active other support of the PD/PI(s) or senior/key personnel since the last reporting period? No changes from the last reporting period.

What other organizations were involved as partners?
Nothing to Report

8. REFERENCES

Datta, A., Loo, S.Y., Huang, B., Wong, L., Tan, S.S., Tan, T.Z., Lee, S.C., Thiery, J.P., Lim, Y.C., Yong, W.P., Lam, Y., Kumar, A.P., Yap, C.T., 2014. SPHK1 regulates proliferation and survival responses in triple-negative breast cancer. Oncotarget 5(15), 5920-5933.

Gao, Y., Gao, F., Chen, K., Tian, M.L., Zhao, D.L., 2015. Sphingosine kinase 1 as an anticancer therapeutic target. Drug Des. Devel. Ther. 9, 3239-3245.

Grenald, S.A., Doyle, T.M., Zhang, H., Slosky, L.M., Chen, Z., Largent-Milnes, T.M., Spiegel, S., Vanderah, T.W., Salvemini, D., 2017. Targeting the S1P/S1PR1 axis mitigates cancer-induced bone pain and neuroinflammation. Pain 158(9), 1733-1742.

Hait, N.C., Avni, D., Yamada, A., Nagahashi, M., Aoyagi, T., Aoki, H., Dumur, C.I., Zelenko, Z., Gallagher, E.J., Leroith, D., Milstien, S., Takabe, K., Spiegel, S., 2015. The phosphorylated prodrug FTY720 is a histone deacetylase inhibitor that reactivates ERalpha expression and enhances hormonal therapy for breast cancer. Oncogenesis 4, e156.

Hait, N.C., Wise, L.E., Allegood, J.C., O'Brien, M., Avni, D., Reeves, T.M., Knapp, P.E., Lu, J., Luo, C., Miles, M.F., Milstien, S., Lichtman, A.H., Spiegel, S., 2014. Active, phosphorylated fingolimod inhibits histone deacetylases and facilitates fear extinction memory. Nat. Neurosci. 17(7), 971-980.

Kharel, Y., Morris, E.A., Congdon, M.D., Thorpe, S.B., Tomsig, J.L., Santos, W.L., Lynch, K.R., 2015. Sphingosine Kinase 2 Inhibition and Blood Sphingosine 1-Phosphate Levels. J Pharmacol Exp Ther 355(1), 23-31.

Maczis, M., Milstien, S., Spiegel, S., 2016. Sphingosine-1-phosphate and estrogen signaling in breast cancer. Adv. Biol. Regul. 60, 160-165.

Nagahashi, M., Yamada, A., Aoyagi, T., Allegood, J., Wakai, T., Spiegel, S., Takabe, K., 2016. Sphingosine-1-phosphate in the lymphatic fluid determined by novel methods. Heliyon 2(12), e00219.

Nagahashi M, Yamada A, Aoyagi T, Huang W-C, Terracina KP, Hait NC, Allegood JC, Tsuchida J, Nakajima M, Katsuta E, Milstien S, Wakai T, **Spiegel S** and Takabe K. Targeting the SphK1/S1P/S1PR1 axis that connects obesity, chronic inflammation, and breast cancer metastasis. Cancer Res. 2017, In revision.

Neuhouser, M.L., Aragaki, A.K., Prentice, R.L., Manson, J.E., Chlebowski, R., Carty, C.L., Ochs-Balcom, H.M., Thomson, C.A., Caan, B.J., Tinker, L.F., Urrutia, R.P., Knudtson, J., Anderson, G.L., 2015. Overweight, Obesity, and Postmenopausal Invasive Breast Cancer Risk: A Secondary Analysis of the Women's Health Initiative Randomized Clinical Trials. JAMA Oncol 1(5), 611-621.

Ruckhaberle, E., Rody, A., Engels, K., Gaetje, R., von Minckwitz, G., Schiffmann, S., Grosch, S., Geisslinger, G., Holtrich, U., Karn, T., Kaufmann, M., 2008. Microarray analysis of altered sphingolipid metabolism reveals prognostic significance of sphingosine kinase 1 in breast cancer. Breast Cancer Res. Treat. 112(1), 41-52.

van der Weyden, L., Arends, M.J., Campbell, A.D., Bald, T., Wardle-Jones, H., Griggs, N., Velasco-Herrera, M.D., Tuting, T., Sansom, O.J., Karp, N.A., Clare, S., Gleeson, D., Ryder, E., Galli, A., Tuck, E., Cambridge, E.L., Voet, T., Macaulay, I.C., Wong, K., Sanger Mouse Genetics, P., Spiegel, S., Speak, A.O., Adams, D.J., 2017. Genome-wide in vivo screen identifies novel host regulators of metastatic colonization. Nature 541(7636), 233-236.

9. APPENDICES

van der Weyden L, Arends MJ, Campbell AD, Bald T, Wardle-Jones H, Griggs N, Velasco-Herrera MD, Tüting T, Sansom OJ, Karp NA, Clare S, Gleeson D, Ryder E, Galli A, Tuck E, Cambridge EL, Voet T, Macaulay IC, Wong K; Sanger Mouse Genetics Project, **Spiegel S**, Speak AO, Adams DJ. Genome-wide in vivo screen identifies novel host regulators of metastatic colonization. Nature. 2017, Jan 12;541(7636):233-236. doi: 10.1038/nature20792.

Keffken K and **Spiegel S**. Sphingosine Kinase 1 in Breast Cancer. Adv. Biol. Regul. 2017, In Press.

LETTER

doi:10.1038/nature20792

Genome-wide *in vivo* screen identifies novel host regulators of metastatic colonization

Louise van der Weyden[1], Mark J. Arends[2], Andrew D. Campbell[3], Tobias Bald[4,5], Hannah Wardle-Jones[1], Nicola Griggs[1], Martin Del Castillo Velasco-Herrera[1], Thomas Tüting[4], Owen J. Sansom[3], Natasha A. Karp[1], Simon Clare[1], Diane Gleeson[1], Edward Ryder[1], Antonella Galli[1], Elizabeth Tuck[1], Emma L. Cambridge[1], Thierry Voet[1,6], Iain C. Macaulay[1], Kim Wong[1], Sanger Mouse Genetics Project†, Sarah Spiegel[7], Anneliese O. Speak[1]* & David J. Adams[1]*

Metastasis is the leading cause of death for cancer patients. This multi-stage process requires tumour cells to survive in the circulation, extravasate at distant sites, then proliferate; it involves contributions from both the tumour cell and tumour microenvironment ('host', which includes stromal cells and the immune system[1]). Studies suggest the early steps of the metastatic process are relatively efficient, with the post-extravasation regulation of tumour growth ('colonization') being critical in determining metastatic outcome[2]. Here we show the results of screening 810 mutant mouse lines using an *in vivo* assay to identify microenvironmental regulators of metastatic colonization. We identify 23 genes that, when disrupted in mouse, modify the ability of tumour cells to establish metastatic foci, with 19 of these genes not previously demonstrated to play a role in host control of metastasis. The largest reduction in pulmonary metastasis was observed in sphingosine-1-phosphate (S1P) transporter spinster homologue 2 (*Spns2*)-deficient mice. We demonstrate a novel outcome of S1P-mediated regulation of lymphocyte trafficking, whereby deletion of *Spns2*, either globally or in a lymphatic endothelial-specific manner, creates a circulating lymphopenia and a higher percentage of effector T cells and natural killer (NK) cells present in the lung. This allows for potent tumour cell killing, and an overall decreased metastatic burden.

To identify microenvironmental genes that regulate metastatic colonization, we performed an 'experimental metastasis assay' involving intravenous injection of B16-F10 mouse metastatic melanoma cells, used previously in the development of checkpoint inhibitors such as CTLA4 and PD-1 (refs 3, 4), and the assessment of pulmonary colonization (Fig. 1a). The 810 mutant mouse lines we assayed were randomly selected and cover a diverse range of molecular functions (Extended Data Fig. 1a and Supplementary Table 1). Using a stringent two-stage selection process, we identified 23 mutant lines showing significantly decreased or increased numbers of pulmonary melanoma foci, defined as a ratio of ≤ 0.6 or ≥ 1.6 and $P \leq 0.0175$ (Mann–Whitney test) for mutant mice versus wild types assayed concurrently (in the initial cohort assayed (Fig. 1a)), and $P < 0.01$ in an integrative data analysis performed on three or more additional cohorts (Supplementary Table 2 and Methods). Since these strains were extensively phenotyped[5], we were able to determine that alterations of immune-related phenotypic traits featured prominently in these 23 mutant lines (Fig. 1b), highlighting the key role of the immune system in microenvironmental regulation of metastasis.

Of the eight genes identified as suppressors of pulmonary metastases, two were members of the interferon regulatory family (IRF), important for immune function; loss of *Irf1* or *Irf7* increased pulmonary metastasis (as well as extra-pulmonary metastases in $Irf1^{tm1a/tm1a}$ mice), probably related to defects in their type-I interferon (IFN)-dependent response[6,7]. In contrast, *Irf5*-deficient mice, with their largely intact type-I IFN response[8], showed no altered pulmonary metastasis phenotype (Extended Data Fig. 1b–f). Similarly, the increased metastasis seen in the p110 catalytic subunit of phosphoinositide 3-kinase (*Pik3cg*)-deficient mice may be related to the critical function of this gene in multiple aspects of T cell, NK cell and neutrophil function[9,10], and the increased metastasis seen in immunoglobulin heavy chain 6 (*Ighm*)-deficient mice is probably due to their multiple immune system abnormalities[11]. In contrast, very little is known about the other four genes we identified as microenvironmental suppressors of metastasis, namely *Abhd17a*, *Dph6*, *Slc9a3r2* and *Rnf10*, which represent novel factors for further studies. Of the 15 mutant mouse lines we identified as having decreased pulmonary melanoma colonies, only four have been previously described as having roles in regulating metastasis: *Entpd1 (Cd39)*, *Nbeal2*, *Cybb* and *Hsp90aa1*, contributing to regulatory T-cell control of NK cells[12], platelet α-granule function[13], generation of phagocyte-derived oxygen radicals[14] and the chaperoning of client proteins involved in tumour progression[15], respectively.

We focused on the S1P transporter *Spns2*, as $Spns2^{tm1a/tm1a}$ mice showed the greatest suppression in the number of pulmonary metastatic melanoma foci, with $Spns2^{tm1a/+}$ mice showing an intermediate phenotype (Fig. 2a). Further, $Spns2^{tm1a/tm1a}$ mice showed reduced numbers of foci in the lungs after tail vein administration of lung CMT-167, colorectal MC-38 or breast EO771.LMB cancer cells (Fig. 2b), and decreased spontaneous pulmonary metastasis (both in number and size of metastatic foci) after subcutaneous administration of HCmel12–mCherry melanoma cells (Fig. 2c and Extended Data Fig. 2a). In contrast, there was no difference in the growth rate of the primary tumour between wild-type and $Spns2^{tm1a/tm1a}$ mice, either for HCmel12–mCherry or B16-BL6 melanoma cells, and no difference in the spontaneous incidence of cancer in aged wild-type and $Spns2^{tm1a/tm1a}$ mice (Extended Data Fig. 2b–d). Tail vein administration of transformed melanocyte WT31 cells (Fig. 2d) and intra-splenic administration of B16-F10 cells (Fig. 2e) resulted in a reduced number of foci in the livers of $Spns2^{tm1a/tm1a}$ mice, suggesting that resistance to metastatic colonization is not pulmonary-restricted.

S1P is a bioactive lipid mediator that plays important roles in diverse cellular functions such as cell proliferation, differentiation, migration and tumorigenesis[16]. Previous studies have shown that SPNS2 functions as a cell-surface S1P transporter that allows intracellular S1P to be secreted into the blood and lymph[17–19]. In agreement with

[1]Wellcome Trust Sanger Institute, Wellcome Genome Campus, Cambridge CB10 1SA, UK. [2]University of Edinburgh Division of Pathology, Edinburgh Cancer Research UK Cancer Centre, Institute of Genetics & Molecular Medicine, Edinburgh EH4 2XR, UK. [3]Cancer Research UK Beatson Institute, Glasgow G61 1BD, UK. [4]Department of Dermatology, University Hospital Magdeburg, Magdeburg 39120, Germany. [5]Department of Immunology in Cancer and Infection Laboratory, QIMR Berghofer Medical Research Institute, Herston 4006, Australia. [6]Department of Human Genetics, University of Leuven (KU Leuven), Leuven, 3000, Belgium. [7]Department of Biochemistry and Molecular Biology, Virginia Commonwealth University School of Medicine, Richmond, Virginia 23298-0614, USA.

*These authors contributed equally to this work.

†Lists of participants and their affiliations appear in the Supplementary Information.

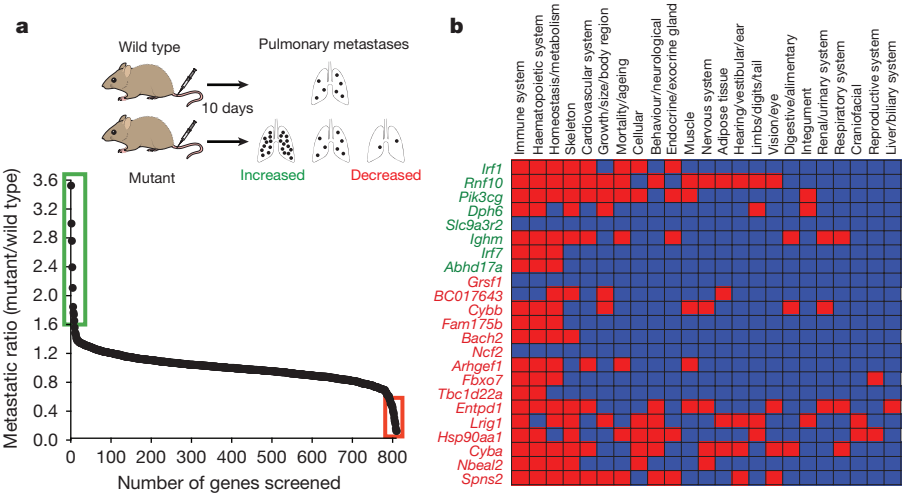

Figure 1 | Identification of microenvironmental regulators of metastatic colonization of the lung. a, Experimental model (schematic) and results from stage 1 of the screen: experimental metastasis assay performed on 810 mutant mouse lines (detailed in the Extended Methods). Those lines with a metastatic ratio of $\leq$0.6 (red box) or $\geq$1.6 (green box) and Mann–Whitney test $P \leq 0.0175$ were taken forward to stage 2 as detailed in Methods. **b**, Top-level mammalian phenotype ontology terms for the 23 statistically significant genes following an integrative data analysis of experimental metastasis assay results from three or more additional cohorts (green is increased metastasis and red is decreased). In the heatmap, red boxes indicate a phenodeviant call, and blue no phenotype annotated (either no phenotype detected or not assayed) as detailed in Methods.

previous studies[17,19], S1P was decreased in serum and increased in lungs of *Spns2*$^{tm1a/tm1a}$ mice (Extended Data Fig. 3a, b). Although extracellular S1P is a key regulator of endothelial barrier homeostasis[20], vascular permeability/extravasation of Evans Blue dye in *Spns2*$^{tm1a/tm1a}$ mice was the same as in controls (Extended Data Fig. 3c), as was the arrival of B16-F10 cells in the lung 90 min after tail vein administration (Extended Data Fig. 3d). However, a significant increase in the number of pulmonary B16-F10 cells showing evidence of apoptosis was observed after 12 h (Extended Data Fig. 3e), suggesting that the lungs of *Spns2*$^{tm1a/tm1a}$ mice represent a hostile environment for tumour cell engraftment. RNA sequencing (RNA-seq) analysis comparing viable B16-F10 cells isolated from lungs 24 h after their administration identified nine differentially expressed (upregulated) genes (Supplementary Table 3); six of these genes (*Pla2g16*, *Epsti1*, *Traf1*, *Glipr2*, *Marcksl1* and *Ccl5*) are known to be involved in pro-metastatic phenotypes of tumour cells, and H2-Q7-positive B16 cells have been shown to be targeted by both NK and cytotoxic T cells[21]. Thus, the transcriptional profile of B16-F10 cells from *Spns2*$^{tm1a/tm1a}$ lungs suggests they are upregulating genes to facilitate their survival in a hostile environment, while at the same time provoking activation of the immune system.

One of the most notable effects of S1P is the regulation of lymphocyte trafficking[22]. SPNS2 has been reported to function as an S1P transporter in endothelial cells but not in erythrocytes or platelets[17]. In agreement with others[17–19,23], *Spns2*$^{tm1a/tm1a}$ mice have a profound reduction in circulating T and B cells, with all other leukocyte (including NK cells) and blood cell lineages unaffected (Extended Data Fig. 4a–c). In the lung, the percentage of T cells was significantly reduced with a small reduction in the B cell percentage and increased NK cells (Fig. 3a), with similar phenotypes observed in the liver (Extended Data Fig. 4d). Consistent with *Spns2* expression in endothelial cells[17], bone marrow chimaeras showed a lymphocyte and metastatic colonization phenotype identical to the genotype of the host (Fig. 3b and Extended Data Fig. 4e, f), confirming that non-haematopoietic stroma regulates these observations. Expression of *Spns2* by endothelial cells is required for the maintenance of an S1P gradient in the lymph that is critical for regulating lymphocyte circulation[18]. In agreement with this, we showed that mice with lymphatic endothelial cell (LEC)-specific deletion of *Spns2* (*Spns2*$^{tm1c/tm1c}$; *Lyve1*$^{cre/+}$ mice) did not have altered serum or lung S1P levels (Extended Data Fig. 5a, b), yet displayed lymphopenia in the blood (Fig. 3c), lungs (Fig. 3d) and other tissues examined (Extended Data Fig. 5c). Critically, this resulted in a decreased number of pulmonary metastasis in *Spns2*$^{tm1c/tm1c}$; *Lyve1*$^{cre/+}$ mice administered either B16-F10 or MC-38 cells (Fig. 3e and Extended Data Fig. 5d).

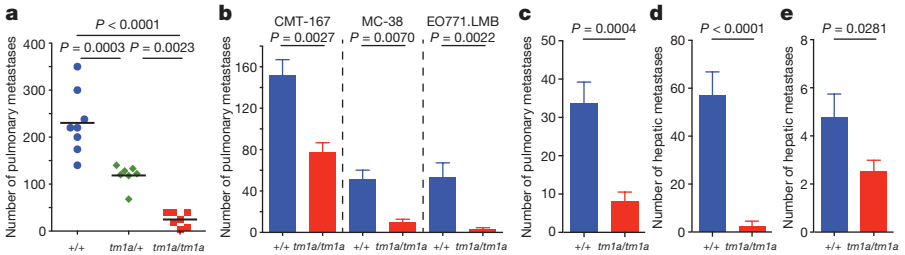

Figure 2 | Ability of *Spns2*-deficient mice to regulate metastatic colonization. a, Experimental metastasis assay using B16-F10 cells in +/+ (blue), *tm1a*/+ (green) or *tm1a/tm1a* (red) male mice. **b**, Experimental metastasis assay using CMT-167 (+/+, $n = 8$; *tm1a/tm1a*, $n = 6$ female mice), MC-38 (+/+, $n = 10$; *tm1a/tm1a*, $n = 5$ male mice) and EO771.LMB cells (+/+, $n = 12$; *tm1a/tm1a*, $n = 5$ female mice). **c**, Spontaneous metastasis assay using HCmel12–mCherry melanoma cells in male mice ($n = 10$ per genotype). **d**, Experimental metastasis assay using WT31 transformed melanocytes in +/+($n = 18$) and *tm1a/tm1a* ($n = 6$) male mice. **e**, Intra-splenic administration of B16-F10 cells in +/+ ($n = 16$) and *tm1a/tm1a* ($n = 15$) female mice. Shown are representative data from two (**b**, CMT-167) or three independent experiments (**a**, **b** (MC-38 and EO771.LMB), **d**) or cumulative results of two independent experiments (**c**, **e**) with mean ± s.e.m. (**b**–**e**) or symbols representing individual mice with horizontal bar at the mean (**a**). *P* values are indicated from one-way analysis of variance (ANOVA) with Šídák's multiple comparisons adjusting for multiple testing (**a**), Mann–Whitney test (**b**–**d**) or one-tailed unpaired *t*-test (**e**).

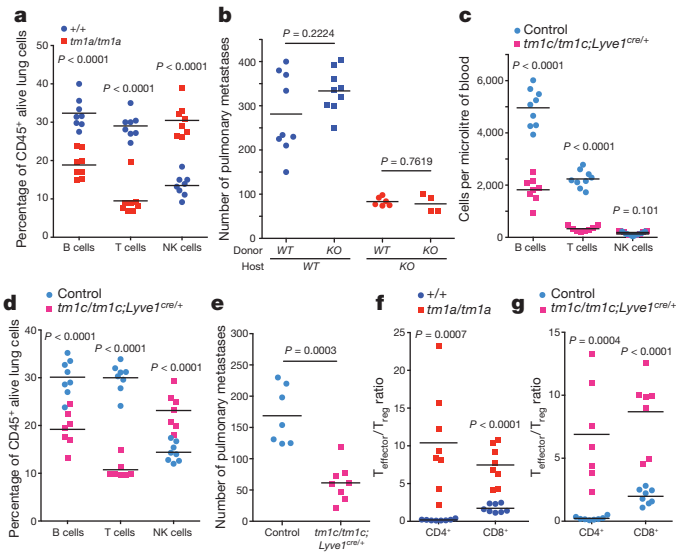

Figure 3 | Characterization of the lymphocyte composition and phenotype in *Spns2*-deficient mice. a, The percentage of lymphocyte subsets in the lungs of +/+ and *tm1a/tm1a* female mice. **b**, Number of metastases in B16-F10-dosed male bone marrow chimaeras (genotypes: +/+ (WT) and *tm1a/tm1a* (KO)). **c**, Numbers of lymphocytes in the blood of control and *tm1c/tm1c; Lyve1*$^{cre/+}$ male mice. **d**, The percentage of lymphocyte subsets in the lungs of control and *tm1c/tm1c; Lyve1*$^{cre/+}$ male mice. **e**, Experimental metastasis assay using B16-F10 cells in control and *tm1c/tm1c; Lyve1*$^{cre/+}$ female mice. **f**, **g**, Effector:regulatory T-cell ratio in the lungs of +/+ and *tm1a/tm1a* female mice or control and *tm1c/tm1c; Lyve1*$^{cre/+}$ male mice. Shown are representative data from two (**b**) or three independent experiments (**a**, **c**–**g**) with symbols representing individual mice with horizontal bar at the mean. *P* values are indicated from two-tailed unpaired *t*-test adjusted by the Holm–Šídák method with α set to 5% (**a**, **c**–**d**, **f**, **g**) or Mann–Whitney test (**b**, **e**).

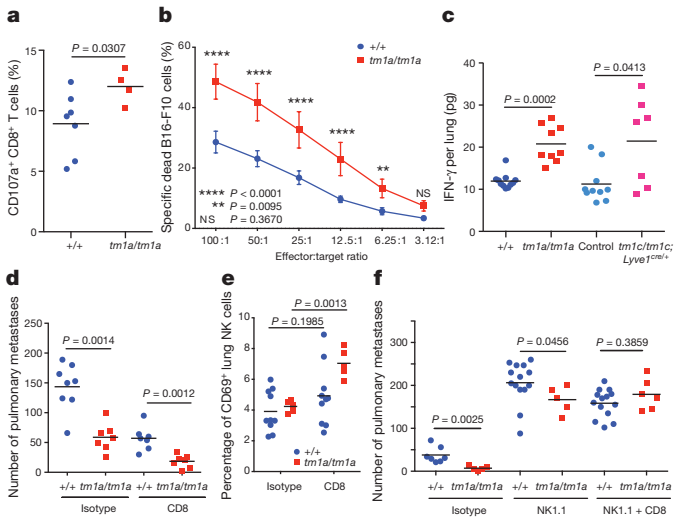

Figure 4 | Lymphocyte regulation of metastatic colonization in *Spns2*-deficient mice. a, Degranulation assay on pulmonary leukocytes from B16-F10-stimulated +/+ and *tm1a/tm1a* female mice in response to *in vitro* re-stimulation with B16-F10. **b**, Cytotoxicity assay on pulmonary leukocytes from B16-F10-stimulated +/+ and *tm1a/tm1a* female mice ($n = 8$ per genotype). **c**, Measurement of IFN-γ in lungs of B16-F10-stimulated +/+ and *tm1a/tm1a* female mice, and control and *tm1c/tm1c; Lyve1*$^{cre/+}$ male mice. **d**, Experimental metastasis assay using B16-F10 cells in +/+ and *tm1a/tm1a* female mice treated with either isotype or anti-CD8 antibody. **e**, The proportion of activated (CD69$^+$) NK cells present in the lungs of +/+ and *tm1a/tm1a* female mice dosed with isotype or anti-CD8 antibody. **f**, Experimental metastasis assay using B16-F10 cells in +/+ and *tm1a/tm1a* male mice treated with isotype, anti-NK1.1 or anti-NK1.1 and CD8 antibody. Shown are representative data from three independent experiments, with symbols representing individual mice with horizontal bar at the mean (**a**, **c**–**f**) or mean ± s.e.m. (**b**). *P* values are indicated from two-tailed unpaired *t*-test with Welch's correction (**a**, **c**, **e**), two-way repeated measures ANOVA with Šídák's multiple comparisons test for each effector:target ratio (**b**) or Mann–Whitney test (**d**, **f**).

We next set out to establish the contribution of SPNS2 to the pulmonary immune microenvironment. S1P–S1PR1 signalling is essential for the recirculation of naive T cells; however, memory T cells downregulate S1PR1 expression and rely on chemokine receptors for trafficking[24]. In contrast, NK cell trafficking in response to S1P requires S1PR5 not S1PR1 (ref. 25). In agreement with this differential requirement of S1P for trafficking, *Spns2*$^{tm1a/tm1a}$ mice showed a significantly higher percentage of anti-tumoural effector memory T cells (CD44^{hi}CD62L^{lo}) relative to immune suppressive regulatory T cells (CD4$^+$CD25$^+$), thus providing an enhanced effector:regulatory T cell ratio (Fig. 3f and Extended Data Fig. 6a, b), with the same observed in *Spns2*$^{tm1c/tm1c}$; *Lyve1*$^{cre/+}$ mice (Fig. 3g and Extended Data Fig. 6c, d). An increased proportion of activated T cells (KLRG1$^+$, CD69$^+$ and CXCR3$^+$) were also observed in the lungs of *Spns2*$^{tm1a/tm1a}$ and *Spns2*$^{tm1c/tm1c}$; *Lyve1*$^{cre/+}$ mice (Extended Data Fig. 6e, f), with a similar phenotype seen in the liver (Extended Data Fig. 7).

Based on this activated phenotype, we performed *ex vivo* re-stimulation assays, where T cells were isolated from the lungs of *Spns2*$^{tm1a/tm1a}$ and control mice 5 days after *in vivo* activation with B16-F10 cells. Using pharmacological stimulation, both CD4$^+$ and CD8$^+$ T cells from *Spns2*$^{tm1a/tm1a}$ mice showed an enhanced degranulation response (cell surface expression of CD107a/LAMP1), and increased intracellular interferon-γ (IFN-γ) relative to control mice (Extended Data Fig. 8a, b). Interestingly, only CD8$^+$ T cells demonstrated enhanced degranulation when co-cultured with B16-F10 cells *ex vivo* suggestive of the presence of an improved antigen-specific response towards B16-F10 (Fig. 4a). This functionally resulted in enhanced B16-F10 target cell killing in an *ex vivo* cytotoxicity assay (Fig. 4b), and increased IFN-γ in lung lysates from B16-F10-stimulated *Spns2*$^{tm1a/tm1a}$ and *Spns2*$^{tm1c/tm1c}$; *Lyve1*$^{cre/+}$ mice (Fig. 4c). Similarly, increased IFN-γ was also observed in lung lysates from MC-38-stimulated *Spns2*$^{tm1a/tm1a}$ mice (Extended Data Fig. 8c) indicating that this is not a B16-F10 restricted phenomenon. Although there was a significant increase in the relative proportion of NK cells in the lung, no difference in NK cell function could be observed *ex vivo* in *Spns2*$^{tm1a/tm1a}$ mice (Extended Data Fig. 8a, b), in agreement with normal NK cell KLRG1, CD69 and CXCR3 expression in both *Spns2*$^{tm1a/tm1a}$ and *Spns2*$^{tm1c/tm1c}$; *Lyve1*$^{Cre/+}$ mice (Extended Data Fig. 8d, e).

To determine whether the beneficial effects of *Spns2* in regulating metastatic colonization could be mediated by CD8$^+$ T cells, we performed *in vivo* depletion experiments using anti-CD8 antibodies. However, paradoxically, depletion of CD8$^+$ T cells (or all T and B cells, such as in *Rag1* knockout mice) has previously been shown to decrease B16-F10 pulmonary metastasis (but not primary tumour growth); this phenomenon has been explained by the 'pro-tumoural' phenotype of CD8$^+$ T cells before tumour cell exposure versus the 'anti-tumoural' effect of antigen-specific CD8$^+$ T cells[26]. Indeed, we replicated this finding observing decreased pulmonary B16-F10 metastases in CD8$^+$ T-cell-depleted wild-type mice (Fig. 4d; and *Rag2* knockout mice, Extended Data Fig. 9); however, a genotype-specific effect was still observed in *Spns2*$^{tm1a/tm1a}$ mice, suggesting the involvement of additional cell types in the regulation of metastatic colonization. Given that we observed compensatory NK cell activation (CD69$^+$) in the lungs of CD8$^+$ T-cell-depleted *Spns2*$^{tm1a/tm1a}$ mice (Fig. 4e), we hypothesized NK cells could be responsible for the significantly reduced metastasis count compared with wild types. To explore this observation further, we performed NK cell depletion, resulting in increased B16-F10 metastases as reported previously[26]; however, *Spns2*$^{tm1a/tm1a}$ mice still showed a significantly reduced number of metastatic foci compared with

wild types (Fig. 4f), in agreement with the enhanced $CD8^+$ response to B16-F10 cells observed *ex vivo* (Fig. 4a). To demonstrate the dual cellular identity responsible for protection in *Spns2*$^{tm1a/tm1a}$ we co-depleted NK and $CD8^+$ cells *in vivo* restoring the number of metastatic foci observed in *Spns2*$^{tm1a/tm1a}$ mice to those of wild-type (Fig. 4f). Thus, we demonstrate that both $CD8^+$ T cells and NK cells can contribute to the reduced pulmonary metastatic burden observed in *Spns2*$^{tm1a/tm1a}$ mice. An alteration of lymphatic endothelial cell function or lung sphingolipid levels in *Spns2*-deficient mice may also contribute to the reduced pulmonary metastatic burden we observe.

Finally, we sought to manipulate the S1P axis pharmacologically by inhibiting S1P lyase, which degrades S1P, using 4′-deoxypyridoxine (DOP), a compound previously shown to increase lymphoid tissue S1P levels and induce a circulating lymphopenia[22]. DOP treatment phenocopied the immune and pulmonary metastasis phenotype of *Spns2*$^{tm1a/tm1a}$ mice (Extended Data Fig. 10), further validating the importance of the S1P axis in control of pulmonary metastatic burden. Importantly modulation of SPNS2 could be a more favourable approach than the S1P-blocking antibody Sphingomab[27,28] or the prodrug FTY720 (ref. 24) (which is phosphorylated *in vivo* to a functional antagonist of S1PR1) as these interventions increase regulatory T cell activity, suppress proliferation of effector T cells[29,30] and increase vascular permeability[18]. Furthermore, as lymphatic endothelial cell-specific deletion of *Spns2* is sufficient to regulate lymphocyte circulation to allow a higher percentage of effector T cells and NK cells in the lung (and liver) and more tumour cell killing, targeting SPNS2 is potentially a more promising option for regulating metastatic colonization than existing S1P pathway modulators.

Online Content Methods, along with any additional Extended Data display items and Source Data, are available in the online version of the paper; references unique to these sections appear only in the online paper.

Received 11 September 2015; accepted 15 November 2016.
Published online 4 January 2017.

1. Quail, D. F. & Joyce, J. A. Microenvironmental regulation of tumor progression and metastasis. *Nature Med.* **19,** 1423–1437 (2013).
2. Chambers, A. F. *et al.* Critical steps in hematogenous metastasis: an overview. *Surg. Oncol. Clin. N. Am.* **10,** 243–255 (2001).
3. Blank, C. *et al.* PD-L1/B7H-1 inhibits the effector phase of tumor rejection by T cell receptor (TCR) transgenic $CD8^+$ T cells. *Cancer Res.* **64,** 1140–1145 (2004).
4. van Elsas, A., Hurwitz, A. A. & Allison, J. P. Combination immunotherapy of B16 melanoma using anti-cytotoxic T lymphocyte-associated antigen 4 (CTLA-4) and granulocyte/macrophage colony-stimulating factor (GM-CSF)-producing vaccines induces rejection of subcutaneous and metastatic tumors accompanied by autoimmune depigmentation. *J. Exp. Med.* **190,** 355–366 (1999).
5. White, J. K. *et al.* Genome-wide generation and systematic phenotyping of knockout mice reveals new roles for many genes. *Cell* **154,** 452–464 (2013).
6. Ogasawara, K. *et al.* Requirement for IRF-1 in the microenvironment supporting development of natural killer cells. *Nature* **391,** 700–703 (1998).
7. Honda, K. *et al.* IRF-7 is the master regulator of type-I interferon-dependent immune responses. *Nature* **434,** 772–777 (2005).
8. Purtha, W. E., Swiecki, M., Colonna, M., Diamond, M. S. & Bhattacharya, D. Spontaneous mutation of the *Dock2* gene in *Irf5*$^{-/-}$ mice complicates interpretation of type I interferon production and antibody responses. *Proc. Natl Acad. Sci. USA* **109,** E898–E904 (2012).
9. Sasaki, T. *et al.* Function of PI3Kγ in thymocyte development, T cell activation, and neutrophil migration. *Science* **287,** 1040–1046 (2000).
10. Tassi, I. *et al.* p110γ and p110δ phosphoinositide 3-kinase signaling pathways synergize to control development and functions of murine NK cells. *Immunity* **27,** 214–227 (2007).
11. Kitamura, D., Roes, J., Kühn, R. & Rajewsky, K. A B cell-deficient mouse by targeted disruption of the membrane exon of the immunoglobulin μ chain gene. *Nature* **350,** 423–426 (1991).
12. Sun, X. *et al.* CD39/ENTPD1 expression by $CD4^+Foxp3^+$ regulatory T cells promotes hepatic metastatic tumor growth in mice. *Gastroenterology* **139,** 1030–1040 (2010).
13. Guerrero, J. A. *et al.* Gray platelet syndrome: proinflammatory megakaryocytes and α-granule loss cause myelofibrosis and confer metastasis resistance in mice. *Blood* **124,** 3624–3635 (2014).
14. Okada, F. *et al.* The role of nicotinamide adenine dinucleotide phosphate oxidase-derived reactive oxygen species in the acquisition of metastatic ability of tumor cells. *Am. J. Pathol.* **169,** 294–302 (2006).
15. Kang, B. H. *et al.* Targeted inhibition of mitochondrial Hsp90 suppresses localised and metastatic prostate cancer growth in a genetic mouse model of disease. *Br. J. Cancer* **104,** 629–634 (2011).
16. Takabe, K. & Spiegel, S. Export of sphingosine-1-phosphate and cancer progression. *J. Lipid Res.* **55,** 1839–1846 (2014).
17. Fukuhara, S. *et al.* The sphingosine-1-phosphate transporter Spns2 expressed on endothelial cells regulates lymphocyte trafficking in mice. *J. Clin. Invest.* **122,** 1416–1426 (2012).
18. Mendoza, A. *et al.* The transporter Spns2 is required for secretion of lymph but not plasma sphingosine-1-phosphate. *Cell Reports* **2,** 1104–1110 (2012).
19. Nagahashi, M. *et al.* Spns2, a transporter of phosphorylated sphingoid bases, regulates their blood and lymph levels, and the lymphatic network. *FASEB J.* **27,** 1001–1011 (2013).
20. Wilkerson, B. A. & Argraves, K. M. The role of sphingosine-1-phosphate in endothelial barrier function. *Biochim. Biophys. Acta* **1841,** 1403–1412 (2014).
21. Chiang, E. Y., Henson, M. & Stroynowski, I. Correction of defects responsible for impaired Qa-2 class Ib MHC expression on melanoma cells protects mice from tumor growth. *J. Immunol.* **170,** 4515–4523 (2003).
22. Schwab, S. R. *et al.* Lymphocyte sequestration through S1P lyase inhibition and disruption of S1P gradients. *Science* **309,** 1735–1739 (2005).
23. Nijnik, A. *et al.* The role of sphingosine-1-phosphate transporter Spns2 in immune system function. *J. Immunol.* **189,** 102–111 (2012).
24. Garris, C. S., Blaho, V. A., Hla, T. & Han, M. H. Sphingosine-1-phosphate receptor 1 signalling in T cells: trafficking and beyond. *Immunology* **142,** 347–353 (2014).
25. Walzer, T. *et al.* Natural killer cell trafficking *in vivo* requires a dedicated sphingosine 1-phosphate receptor. *Nature Immunol.* **8,** 1337–1344 (2007).
26. Cuff, S., Dolton, G., Matthews, R. J. & Gallimore, A. Antigen specificity determines the pro- or antitumoral nature of $CD8^+$ T cells. *J. Immunol.* **184,** 607–614 (2010).
27. Ponnusamy, S. *et al.* Communication between host organism and cancer cells is transduced by systemic sphingosine kinase 1/sphingosine 1-phosphate signalling to regulate tumour metastasis. *EMBO Mol. Med.* **4,** 761–775 (2012).
28. Visentin, B. *et al.* Validation of an anti-sphingosine-1-phosphate antibody as a potential therapeutic in reducing growth, invasion, and angiogenesis in multiple tumor lineages. *Cancer Cell* **9,** 225–238 (2006).
29. Liu, G., Yang, K., Burns, S., Shrestha, S. & Chi, H. The S1P(1)-mTOR axis directs the reciprocal differentiation of T(H)1 and T(reg) cells. *Nature Immunol.* **11,** 1047–1056 (2010).
30. Liu, Y. *et al.* The sphingosine-1-phosphate receptor agonist FTY720 and its phosphorylated form affect the function of $CD4^+CD25^+$ T cells *in vitro*. *Int. J. Mol. Med.* **30,** 211–219 (2012).

Supplementary Information is available in the online version of the paper.

Acknowledgements This work was supported by grants from Cancer Research UK (D.J.A. and O.J.S.), the Wellcome Trust (WT098051), Combat Cancer (D.J.A.), the European Research Council (311301 COLONCAN to O.J.S. and A.D.C.), National Institutes of Health U54HG004028 (N.A.K.), and Department of Defense BCRP Program Award W81XWH-14-1-0086 (S.S.). T.T. was funded by project A27N in the SFB854, and T.B. was funded in part by an EMBO Long-Term Fellowship (ALTF 945-2015) and the European Commission (Marie Curie Action LTFCOFUND2013, GA-2013-609409). We thank J. Allegood for sphingolipid analyses and acknowledge the VCU Lipidomics Core, which is supported in part by funding from the National Institutes of Health–National Cancer Institute (NIH–NCI) Cancer Center Support Grant P30CA016059, V. Iyer (Wellcome Trust Sanger Institute) for bioinformatics analysis, and members of the Wellcome Trust Sanger Institute Research Support Facility for their care of the mice.

Author Contributions L.v.d.W. devised and implemented the pulmonary metastasis screen, performing all the primary screen, confirmation and characterization studies. M.J.A. analysed the histopathological sections. A.D.C. and O.J.S. performed and analysed the intrasplenic B16-F10 assays. T.B. and T.T. performed and analysed the spontaneous metastasis assay. H.W.-J. and N.G. managed mouse breeding and were responsible for issuing phenotyping cohorts. M.D.C.V.-H., T.V., I.C.M. and K.W. performed the RNA-seq analysis. D.G. and E.R. genotyped the mice and performed gene expression analysis. S.C., A.G., E.T. and E.L.C. performed additional phenotypic characterization. The Sanger Mouse Genetics Project generated and phenotyped the mice as part of a primary phenotyping pipeline. S.S. oversaw the lipidomic analysis and provided input to the project and the manuscript. A.O.S. devised, performed and analysed the immunophenotyping assays. L.v.d.W., A.O.S. and D.J.A. led the project. L.v.d.W., A.O.S. and D.J.A. wrote the manuscript with contributions from all authors.

Author Information Reprints and permissions information is available at www.nature.com/reprints. The authors declare no competing financial interests. Readers are welcome to comment on the online version of the paper. Correspondence and requests for materials should be addressed to L.v.d.W. (lvdw@sanger.ac.uk) or D.J.A. (da1@sanger.ac.uk).

Reviewer Information *Nature* thanks C. Ghajar and the other anonymous reviewer(s) for their contribution to the peer review of this work.

METHODS

Mice. The generation and genotyping of *Spns2*$^{tm1a(KOMP)Wtsi}$ (referred to as *tm1a/tm1a*)[23], *Lyve1*$^{tm1.1(EGFP/cre)Cys/J}$ (referred to as *Lyve1*^{cre}) mice[31] and *Rag2*^{tm1Fwa} mice[32] have been described previously. *Spns2*$^{tm1c(KOMP)Wtsi}$ (referred to as *tm1c/tm1c*) mice were generated from crossing *Spns2*$^{tm1a(KOMP)Wtsi}$ mice with Flp-deleter mice[33] and crossed to *Lyve1*^{cre} mice to generate experimental mice (*tm1c/tm1c*; *Lyve1*$^{cre/+}$) with littermates used as controls (*tm1c/+*; *Lyve1*$^{+/+}$ and *tm1c/tm1c*; *Lyve1*$^{+/+}$; referred to as 'controls'). The care and use of all mice in this study were in accordance with the UK Animals in Science Regulation Unit's Code of Practice for the Housing and Care of Animals Bred, Supplied or Used for Scientific Purposes, the Animals (Scientific Procedures) Act 1986 Amendment Regulations 2012, and all procedures were performed under a UK Home Office Project licence, which was reviewed and approved by the Sanger Institute's Animal Welfare and Ethical Review Body (unless otherwise stated). Housing and husbandry conditions were as described previously[34], with the exceptions that a cage density of one to six mice per cage was used and mice were maintained on Mouse Breeders Diet (Laboratory Diets, 5021-3) throughout the study. Unless specified otherwise, all mice were used at 6–12 weeks of age.

General experimental design. For most experiments, random allocation to treatment group was achieved through the process of Mendelian inheritance, with age- and sex-matched mice being selected across different litters and matings (to minimize potential litter and/or cage effects). The two exceptions were the NK cell depletion study and bone marrow chimaera study: in these studies, Mendelian inheritance was used to randomize assignment of animals to a genotype group; then, within this block, alternate allocation was used to assign treatment. Unless specified otherwise, the researcher was not blinded to the identity of the genotype and/or treatment of a mouse during any procedures because these were written on the cage card. Pilot experiments were performed to determine sample size with adequate statistical power for all studies except the high throughput screen where this this was not possible owing to the scale of breeding that would be required. For each procedure, exclusion criteria used are listed where applicable in the materials and methods. If no exclusion criteria are detailed, all data were included. The manuscript was prepared to meet ARRIVE reporting guidelines[35].

Cell lines. The mouse melanoma B16-F10 cell line was purchased from ATCC (CRL-6475) and the highly metastatic mouse melanoma B16-BL6 cell line was purchased from the University of Texas, MD Anderson Cancer Center and authenticated by whole genome and transcriptome sequencing. The mouse lung carcinoma CMT-167 cell line was purchased from Sigma-Aldrich (10032302) and the other cell lines were obtained from the laboratories that generated them. Specifically, the metastatic mouse colorectal MC-38 cell line[36] was a gift from L. Borsig (University of Zurich, Switzerland), the metastatic mouse mammary cancer EO771.LMB cell line[37] was a gift from R. L. Anderson (Peter MacCallum Cancer Centre, Australia), the metastatic HCmel12–mCherry melanoma cell line[38] was a gift from T. Tuting (University Hospital Magdeburg, Germany) and the transformed mouse melanocyte WT31 cell line (*Tyr::Nras*$^{Q61K/°}$; *INK4a*$^{-/-}$)[39] was a gift from O. Sansom (Beatson Institute for Cancer Research, Scotland). None of the cell lines used appears in the International Cell Line Authentication Committee database. All cells (apart from WT31 cells) were maintained in DMEM with 10% (v/v) fetal calf serum and 2 mM glutamine, 100 U/mL penicillin/streptomycin (with the addition of 20 mM HEPES for EO771.LMB cells) at 37 °C, 5% CO_2. WT31 cells were maintained in RPMI with 10% (v/v) fetal calf serum and 2 mM glutamine, 100 U/mL penicillin/streptomycin at 37 °C, 5% CO_2. All cell lines were screened for the presence of mycoplasma and mouse pathogens (at Charles River Laboratories, USA) before culturing and never cultured for more than five passages. The B16-F10–mCherry cells, stably expressing mCherry, were generated by co-transfection of B16-F10 cells with 4.5 μg of PB-CAGG-LUC-2A–mCherry–PURO-PB plasmid (a gift from D. Ryan, Wellcome Trust Sanger Institute) and 0.5 μg of PBase-expressing plasmid using Fugene HD (Promega) according to the manufacturer's recommendations. After selection in 5 μg/mL puromycin (Gibco BRL) for 10 days, cell sorting was performed (MoFlo XDP, Beckman Coulter) to select for those cells expressing high levels of mCherry and was maintained in 5 μg/mL puromycin.

Experimental metastasis assay. B16-F10 (4×10^5), CMT-167 (1×10^5), MC-38 (4×10^5), EO771.LMB (4×10^5) or WT31 (2.5×10^6) cells resuspended in 0.1 mL phosphate buffered saline (PBS) were injected into the tail vein of 6- to 12-week-old sex-matched syngeneic control and mutant mice. After 10 days (or 30 days if WT31 cells were used) the mice were killed, their lungs removed (or livers removed if WT31 cells were used) and the number of metastatic foci counted macroscopically (for B16-F10 and WT31 cells) or microscopically from formalin-fixed haematoxylin and eosin-stained sections by a pathologist (for CMT-167, MC-38 and EO771.LMB cells; the pathologist was blinded to the genotypes of the samples). For intrasplenic injections of B16-F10 melanoma cells, the mice were anaesthetized under isofluorane gas and a laparotomy performed to expose the spleen. B16-F10 cells (1×10^4) resuspended in 0.03 mL PBS were injected into the tail of the spleen, after which surgical incisions were sutured and surgical clips applied. Animals were monitored throughout recovery with dietary support and analgesia (Rimadyl 100 μg/mL *ad libitum*) provided, as approved by the Glasgow University Ethics Committee. After 14 days, the mice were killed, their livers removed and the number of metastatic foci counted macroscopically.

Metastatic colonization screen. The experimental metastasis assay (detailed above) was performed by administering 4×10^5 B16-F10 cells to age- and sex-matched wild-type and mutant mice. The mice were 6–12 weeks old (typically 6–8 weeks) at time of dosing and dosing cohorts typically consisted of 12–24 control mice with 3–5 different mutant alleles being screened (3–8 mutant mice per allele). To ensure consistency, preparation of the cells, administration into the tail vein and counting of pulmonary metastatic foci were performed by the same individual. To ensure a high level of accuracy, a two-stage process was implemented, with final calls only being made after data had been collected from multiple independent cohorts (the data from all mice were included in the analysis except for when the full 0.1 mL of cell suspension were not successfully administered because of difficulties at the time of injection). The first stage was a high-throughput process to identify lines of potential interest for the second stage; in this stage, mutant lines with a 'metastatic ratio' (mean number of metastatic foci in the mutant cohort divided by mean number of metastatic foci in the wild-type cohort) ≤ 0.6 or ≥ 1.6 and $P \leq 0.0175$ in the Mann–Whitney test (a subsequent analysis estimated a false discovery rate of 15%) progressed to the second stage. In the second stage, at least three additional cohort(s) of mice (of both sexes) were independently studied and the data combined into an integrative data analysis (IDA) as detailed in the Statistics section.

Bone-marrow chimaeras. Wild-type (CD45.1 congenically marked syngeneic) and *tm1a/tm1a* mice were given 2 × 4.2 Gy whole-body irradiation followed by tail vein administration of 3×10^6 bone marrow cells from either wild-type (CD45.1 congenic) or *tm1a/tm1a* mice. Six weeks after transplantation, a tail vein blood sample was taken from the mice to assess the relative proportion of CD45.1 versus CD45.2 cells and the number of T and B lymphocytes present in the peripheral blood; 2 days later, an experimental metastasis assay was performed.

***In vivo* depletion studies.** Mice were given intraperitoneal doses of antibodies (anti-CD8 (clone YTS169.4), rat IgG2b isotype control (clone LTF-2), anti-NK1.1 (clone PK136), mouse IgG2a (clone C1.18.4)), 200 μg in 0.1 mL PBS on days −3, 0 and +5, with B16-F10 cells administered by tail vein on day 0 (CD8-depletion mice were dosed with 4×10^5 B16-F10 cells; NK and NK/CD8-depletion mice were dosed with 2×10^5 B16-F10 cells). Tail vein blood samples were collected from all mice on day +1 to confirm the depletion was effective. All antibodies were 'InVivoMAb' from BioXCell.

S1P lyase inhibitor studies. For S1P lyase inhibitor studies, the mice were either given glucose (10 g/L) or glucose plus 4′ deoxypyridoxine (DOP, 30 mg/L; Sigma) in their drinking water 1 week before any experimentation (with mice remaining on treatment for the duration of the experiment)[22].

Primary tumour growth studies. For examination of orthotopic tumour growth, wild-type and *tm1a/tm1a* male and female mice at 6–8 weeks of age were subcutaneously administered 2.5×10^3 B16-BL6 melanoma cells in the flank. The developing tumours were measured every second day and if they had reached (or were very close to) 2 cm^2 on the day of measurement the mice were immediately culled (no tumour was ever more than 2.4 cm^2), as approved by a Home Office Inspector under the authority of the Animals (Scientific Procedures) Act 1986.

Spontaneous metastasis assay. Wild-type and *tm1a/tm1a* mice were subcutaneously dosed with 2×10^5 HCmel12–mCherry melanoma cells and the resulting tumour growth was monitored by inspection and palpation. The size of the tumour was measured weekly using Vernier callipers and recorded as mean diameter. Mice were killed when progressively growing melanomas exceeded 20 mm in size and tissues collected for further analyses (in accordance with institutional and national guidelines for the care and use of laboratory animals with approval by the local government authorities (LANUV, NRW, Germany)). The number of macroscopically visible metastases present on the lung surface were counted by two independent investigators in a blinded fashion.

Preparation of tissue cell suspensions. Mice were perfused with 20 mL PBS by cardiac puncture and the tissues were disrupted in C tubes using program m_lung_01 with an gentleMACS (Miltenyi Biotec) in Hanks Balanced Salt solution (HBSS) containing calcium and magnesium. Liberase DL (Collagenase with low dispase content, Roche, Burgess Hill, UK) was added to a final concentration of 0.1 U/mL and incubated for 30 min at 37 °C. The tubes were then processed using program m_lung_02 and DNase (0.1 mg/mL) was added for a further 30 min at 37 °C. The resulting cell suspension was centrifuged at 400 *g* for 5 min, resuspended in 2 mL fluorescence-activated cell sorting (FACS) buffer (D-PBS without calcium and magnesium containing 2 mM EDTA, 0.5% fetal calf serum and 0.09% sodium azide), passed through a 30 μm cell strainer and analysed on the flow cytometer.

To determine the number or viability of melanoma cells present in the lungs of mice, the mice were dosed with either 1×10^6 B16-F10 cells labelled with 10 μM CFSE (Molecular Probes, Invitrogen) at 90 min before perfusion or 1×10^6 B16-F10–mCherry cells at 12 h before perfusion. In each case, the lung cell suspension was analysed on the flow cytometer. For lung/liver leukocyte analysis, the leukocytes were enriched from other cell types in the cell suspension on a Percoll discontinuous gradient (67.5%/44%) and washed three times with FACS buffer. Single cell suspensions from spleen and lymph nodes (pooled inguinal) were prepared using frosted end of microscope slides in FACS buffer. Red blood cells were lysed from spleen samples by the addition of 2 mL PharmLyse (BD Biosciences) for 90 s at room temperature then stopped by the addition of 10 mL FACS buffer. Both spleen and lymph node samples were passed through a 30 μm cell strainer before staining. 'Naive' mice were those that had not been administered B16-F10 cells and 'stimulated' mice were those that had been tail vein administered B16-F10 cells 3 or 5 days before analysis as indicated in the figure legend.

FACS immunostaining. Samples were blocked with 1 μg of Mouse BD FC Block (anti CD16/32, clone 2.4G2, BD Biosciences) for 10 min before addition of multicolour antibody cocktails using titrated amounts to give saturating binding (see Supplementary Table 4 for more details). After washing, cells were stained with a viability dye (Live/Dead Blue, Invitrogen, 1 in 1,000 dilution in PBS) for 10 min at room temperature, then washed before acquisition. For determination of apoptosis, lung preparations were prepared as above and were stained with Caspglow reagent (eBioscience UK) according to the manufacturer's instructions for 1 h at 37 °C. Cells were washed with Annexin binding buffer and stained with Annexin V-APC (both BD Biosciences) according to the manufacturer's instructions for 15 min at room temperature. Cells were washed with Annexin binding buffer and resuspended Annexin V binding buffer containing 1 μg/mL DAPI (Life Technologies) before acquisition. To determine absolute cell counts of leukocyte populations, whole blood was counted with a haematology analyser (Scil Vetabc) and the white blood cell count was used to derive the number cells per microlitre of blood, with the immune cell populations as percentage of leukocytes.

Lung leukocyte cytotoxicity. Leukocytes were prepared from perfused lungs 5 days after B16-F10 injection as described above. B16-F10 target cells were labelled with 1 μM CFSE (Molecular Probes, Invitrogen). Target cells and lung leukocytes were added to 96-well round-bottomed plates at effector to target ratios indicated for 4 hours at 37 °C in complete DMEM medium (prepared as described in 'Cell lines'). The cells were washed twice with ice-cold PBS then resuspended in 100 μL Live/Dead far red (Invitrogen, 1 in 1,000 dilution in PBS) for 10 min at room temperature. Cells were washed twice and resuspended in BD Cell Fix for 10 min at room temperature and washed twice with FACS buffer, before acquisition where 2,000 target cells were collected. Cytotoxicity was calculated according to the following equation: (percentage of dead target cells with effector cells) – (percentage of dead target cells with no effector cells added).

Leukocyte degranulation and IFN-γ production. Leukocytes were prepared from perfused lungs 5 days after B16-F10 injection as described above. Cells were stimulated with target cells (B16-F10 at effector to target ratio of 2.5:1) or phorbol myristate acetate (PMA) and ionomycin (100 ng/mL and 150 ng/mL, respectively both Sigma-Aldrich). Cells and stimulus were added to 96-well round-bottomed plates in the presence of anti-CD107a antibody and BD GolgiStop (monensin, final concentration 2 μM) in complete DMEM medium for 4 hours at 37 °C. The plates were washed twice with ice-cold FACS buffer before blocking then staining with anti-TCRβ, CD45, NK1.1 and CD8α antibodies. Cells were then stained with a fixable viability indicator (Live/Dead Blue, Invitrogen) before intracellular staining for IFN-γ according to standard methods and analysed by flow cytometry where a minimum of 50,000 $CD45^+$ alive leukocyte events were collected. CD107a and IFN-γ gates were set on unstimulated leukocyte samples and specific degranulation or intracellular IFN-γ staining was calculated by subtracting the leukocyte alone unstimulated values from the treated values.

Flow cytometry. All samples were analysed on an LSR II or LSRFortessa (both BD Biosciences) that were standardized using BD Cytometer Setup and Tracking Beads and software. Compensation was determined using Ultracomp eBeads (eBioscience) for all antibodies, and ArC amide binding beads (Invitrogen) for live/dead stains. Data acquisition was controlled with BD FACSDiva version 6.3 or version 8.0.1 software. For the analysis of B16-F10 apoptosis, a threshold was applied to the mCherry channel (561 nm laser 610/20 BP) to exclude 90% of the lung cells. For the analysis of cytotoxicity, a threshold was applied to the CFSE channel (488 nm laser 530/30 BP) to exclude 90% of the lung leukocytes. In both cases these were established using B16-F10 mCherry- or CFSE-labelled B16-F10 cells. In all other cases an FSC-A threshold was used to exclude debris. All samples were analysed using FlowJo 10.7 and were analysed genotype and/or treatment blind. For all phenotyping data, doublets were excluded using FSC-A versus FSC-H gates, sample acquisition issues (such as clumps and unstable event rate) were excluded using a time gate against a fluorescent parameter that was off the laser with the longest time delay, dead cells were excluded from all tissue analysis using a viability indicator and debris excluded with FSC-A versus SSC-A gates. A leukocyte gate was set with CD45 and SSC-A and all cell subsets are reported as the percentage of this parent gate. T cells were defined as $TCR\gamma\delta^-$ $CD3^+$ $NK1.1^-$ or $TCR\beta^+$ $NK1.1^-$ with $CD4^+$ and $CD8^+$ gates defined on this parent population, NK cells defined as $NK1.1^+$ $CD3^-$ or TCR^-, and B cells defined as $CD19^+$. T and NK cell phenotypes were determined using fluorescent minus one controls to establish gating. Data from a sample were excluded if there were insufficient events in the parent gate to allow analysis: for example, if there were fewer than 50,000 $CD45^+$ alive leukocytes in lung phenotyping data, these were excluded from the data set.

Lung IFN-γ determination. Five days after B16-F10 injection lungs were saline perfused and homogenized in Tris-buffered saline with 0.5% Triton X100 using M tubes and a gentleMACS (Miltenyi Biotec) with program protein_01. Samples were cleared by centrifugation for 10 min at 20,000 *g* at 4 °C. IFN-γ levels in the lung lysates were determined using a Ready Set Go ELISA kit (eBioscience, Hatfield, UK) according to the manufacturer's instructions.

Transcriptome sequencing. Wild-type and *tm1a/tm1a* mice tail vein dosed with 1×10^6 B16-F10–mCherry cells were killed after 24 h and lung cell suspensions prepared as described above. Using a cell sorter (MoFlo XDP), B16-F10–mCherry cells were identified after displaying in a bivariate plot of SSC-log versus mCherry by gating on high forward scatter versus side scatter to exclude some debris and dead cells and positively sorted. RNA was extracted from the sorted cells using the RNeasy Mini kit (Qiagen), according to the manufacturer's instructions, and used to generate cDNA with the Smart-seq2 protocol[40,41]. Multiplexed sequencing libraries were generated from amplified cDNA using Nextera XT (Illumina). The multiplexed mRNaseq libraries were pooled and sequenced across multiple lanes on the Illumina Hiseq 2000 (version 3). Paired-end 100 bp reads were aligned with STAR version 2.3.0 (ref. 42), allowing a minimum (50 bp) and maximum intron size (500,000 bp). STAR genome index files were generated using a GTF file corresponding to gene models from ENSEMBL version 74 and reference genome version GRCm38. Read counting was performed with htseq-count from the HTSeq package (version 0.5.4p5)[43]. The htseq-count software was run with the options 'intersection-nonempty' mode, non-stranded, minimum quality 10, and 'exon' was used as the feature type, with 'gene_id' as the GTF feature ID. The Bioconductor (version 3.1)[44] package DESeq2 (version 1.8.1)[45] was used for differential expression analysis. We used the local fit parameter for dispersion fitting and obtained the significance with the DESeq2 negative binomial Wald test function. Genes with adjusted to $P < 0.05$ after Benjamini–Hochberg correction and a $\log_2$(fold change) less than -0.59 or greater than 0.59 was considered significantly differentially expressed.

Analysis of sphingolipids by LC-ESI-MS/MS. Serum and saline perfused lung tissues were collected from the mice. After the addition of internal standards (0.5 nmol each; Avanti Polar Lipids, Alabaster, Alabama, USA) the lipids were extracted and sphingolipids were quantified by LC-ESI-MS/MS (4000 QTRAP, AB Sciex, Framingham, Massachusetts, USA) as described previously[46].

Statistics. Statistical tests were selected to be appropriate for the data properties (for example, normality or homogeneity of variance) and experimental design such that the assumptions of the test would be met. Where multiple testing occurred within a study, it was managed by controlling the family-wise error rate as detailed in the associated figure legend. Integrative data analysis (also called mega-analysis)[47] was completed using R (package nlme version 3.1), treating each experiment as a fixed effect. An iterative top-down modelling strategy was implemented starting with the most comprehensive model (either equations (1) or (2)) appropriate for the collection strategy implemented and ensuring the model only included terms where they could be independently assessed:

$$Y = \beta_0 + \beta_{1,\ \mathrm{Sex}} + \beta_{2,\ \mathrm{Experiment}} + \beta_{3,\ \mathrm{Genotype}} + \beta_{4,\ \mathrm{Sex*Genotype}} \quad (1)$$

$$Y = \beta_0 + \beta_{2,\ \mathrm{Experiment}} + \beta_{3,\ \mathrm{Genotype}} \quad (2)$$

The optimization process first selected a covariance structure for the residual, then the model was reduced by removing non-significant fixed effects, and finally the genotype effect was tested and model diagnostics visualized. For the hypothesis test of primary interest, the impact of genotype, the per-comparison error rate threshold *P* values were adjusted to account for the multiple comparisons to control the family-wise error rate to 5% using the Hochberg method[48].

Bioinformatic analysis of molecular functions and phenotype. Using the Mouse Genome Informatics (MGI) portal (http://www.informatics.jax.org), all 810 mutant lines screened were separated into unique symbols (to separate out microRNA clusters) and annotated with molecular function using the Gene Ontology (GO) batch query selecting the GO_Slim annotations. Phenotypic information was pulled from MGI as a batch query (MGI 6.06, release date

5 October 2016) and supplemented with annotations from the International Mouse Phenotyping Consortium (IMPC – release 4.3, 26 April 2016) portal (http://www.mousephenotype.org). The reported mammalian phenotype (mp) terms returned were collapsed to the top-level term for the generation of the heatmap. We were not able to discriminate between no phenotype detected and no phenotypic data present; thus both outcomes are represented with a blue cell with the presence of phenotypes indicated by the red cell.

Data availability. The data that support the findings of this study are available from the corresponding author upon reasonable request. The data for Extended Data Fig. 2c are available in the online version of this paper. The data for the results of the experimental metastasis assay from stage 1 of the screen and the integrative data analysis are available in the online version of this paper. All RNA-seq data are available under European Nucleotide Archive accession number ERP005660 and ArrayExpress accession number E-ERAD-287, with the results of the analysis shown in Supplementary Table 3.

31. Pham, T. H. *et al.* Lymphatic endothelial cell sphingosine kinase activity is required for lymphocyte egress and lymphatic patterning. *J. Exp. Med.* **207,** 17–27 (2010).
32. Shinkai, Y. *et al.* RAG-2-deficient mice lack mature lymphocytes owing to inability to initiate V(D)J rearrangement. *Cell* **68,** 855–867 (1992).
33. Kranz, A. *et al.* An improved Flp deleter mouse in C57Bl/6 based on Flpo recombinase. *Genesis* **48,** 512–520 (2010).
34. Karp, N. A. *et al.* Impact of temporal variation on design and analysis of mouse knockout phenotyping studies. *PLoS ONE* **9,** e111239 (2014).
35. Kilkenny, C., Browne, W. J., Cuthill, I. C., Emerson, M. & Altman, D. G. Improving bioscience research reporting: the ARRIVE guidelines for reporting animal research. *PLoS Biol.* **8,** e1000412 (2010).
36. Borsig, L., Wong, R., Hynes, R. O., Varki, N. M. & Varki, A. Synergistic effects of L- and P-selectin in facilitating tumor metastasis can involve non-mucin ligands and implicate leukocytes as enhancers of metastasis. *Proc. Natl Acad. Sci. USA* **99,** 2193–2198 (2002).
37. Johnstone, C. N. *et al.* Functional and molecular characterisation of EO771. LMB tumours, a new C57BL/6-mouse-derived model of spontaneously metastatic mammary cancer. *Dis. Model. Mech*. **8,** 237–251 (2015).
38. Bald, T. *et al.* Ultraviolet-radiation-induced inflammation promotes angiotropism and metastasis in melanoma. *Nature* **507,** 109–113 (2014).
39. Lindsay, C. R. *et al.* P-Rex1 is required for efficient melanoblast migration and melanoma metastasis. *Nature Commun*. **2,** 555 (2011).
40. Picelli, S. *et al.* Smart-seq2 for sensitive full-length transcriptome profiling in single cells. *Nature Methods* **10,** 1096–1098 (2013).
41. Picelli, S. *et al.* Full-length RNA-seq from single cells using Smart-seq2. *Nature Protocols* **9,** 171–181 (2014).
42. Dobin, A. *et al.* STAR: ultrafast universal RNA-seq aligner. *Bioinformatics* **29,** 15–21 (2013).
43. Anders, S., Pyl, P. T. & Huber, W. HTSeq—a Python framework to work with high-throughput sequencing data. *Bioinformatics* **31,** 166–169 (2015).
44. Gentleman, R. C. *et al.* Bioconductor: open software development for computational biology and bioinformatics. *Genome Biol.* **5,** R80 (2004).
45. Love, M. I., Huber, W. & Anders, S. Moderated estimation of fold change and dispersion for RNA-seq data with DESeq2. *Genome Biol.* **15,** 550 (2014).
46. Hait, N. C. *et al.* Regulation of histone acetylation in the nucleus by sphingosine-1-phosphate. *Science* **325,** 1254–1257 (2009).
47. Curran, P. J. & Hussong, A. M. Integrative data analysis: the simultaneous analysis of multiple data sets. *Psychol. Methods* **14,** 81–100 (2009).
48. Hochberg, Y. A sharper Bonferroni procedure for multiple tests of significance. *Biometrika* **75,** 800–802 (1988).

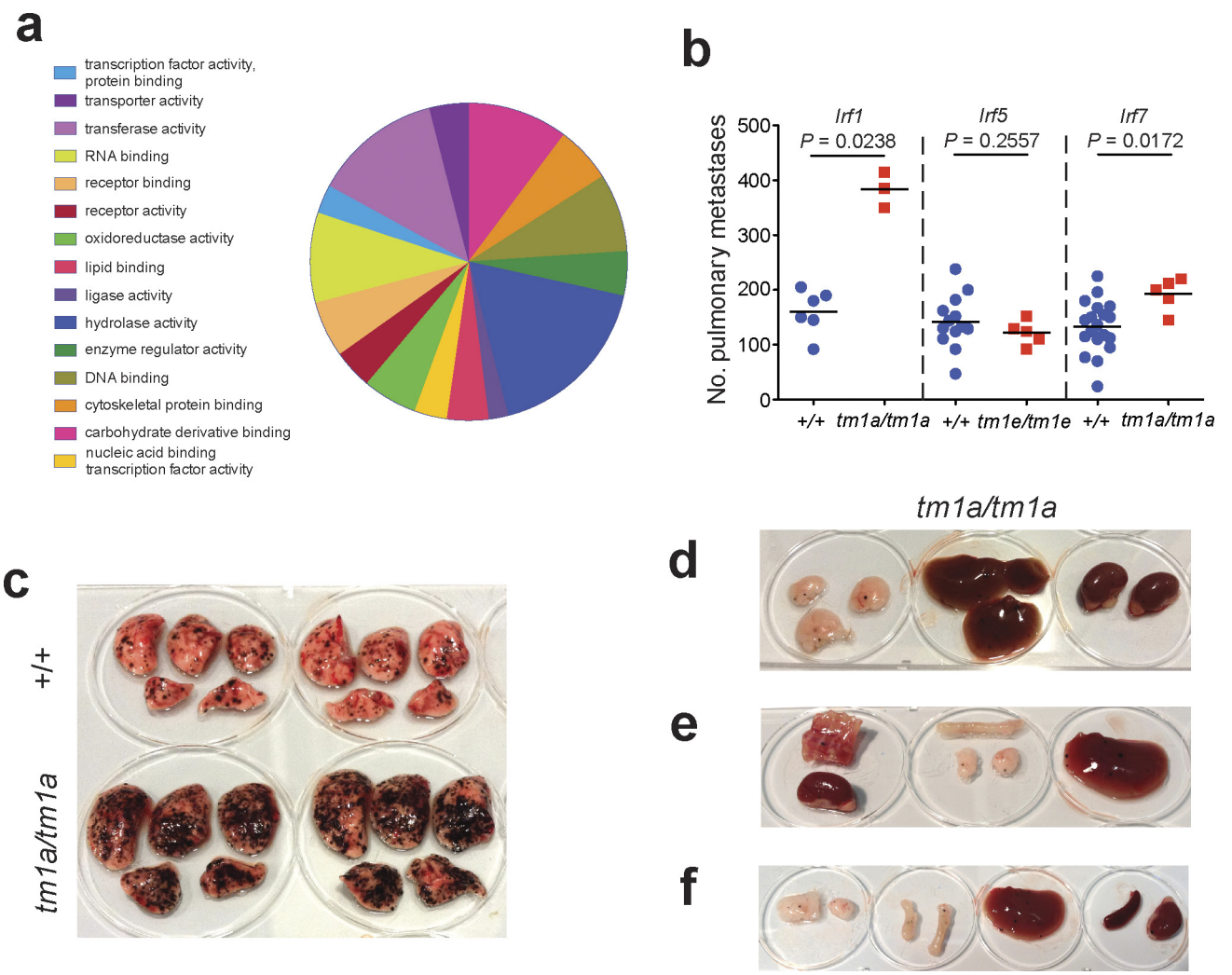

Extended Data Figure 1 | Molecular function of 810 mutant mouse lines screened and phenotypic characterization members of the interferon regulatory factor (*Irf*) family. a, Molecular function Gene Ontology annotation of the 810 mutant mouse lines screened as detailed in Methods. **b**, Experimental metastasis assay using B16-F10 cells in $Irf1^{tm1a/tm1a}$, $Irf5^{tm1e/tm1e}$, $Irf7^{tm1a/tm1a}$ and concurrent control female mice. Shown are representative data from two (*Irf5*), four (*Irf1*) or six (*Irf7*) independent experiments. Symbols represent individual mice with a horizontal bar at the mean. *P* values are from a Mann–Whitney test. **c–f**, Representative photographs showing B16-F10 metastatic colonies on the (**c**) lungs of +/+ and $Irf1^{tm1a/tm1a}$ mice and (**d–f**) the presence of extra-pulmonary metastases in $Irf1^{tm1a/tm1a}$ mice (tissues from three mice shown).

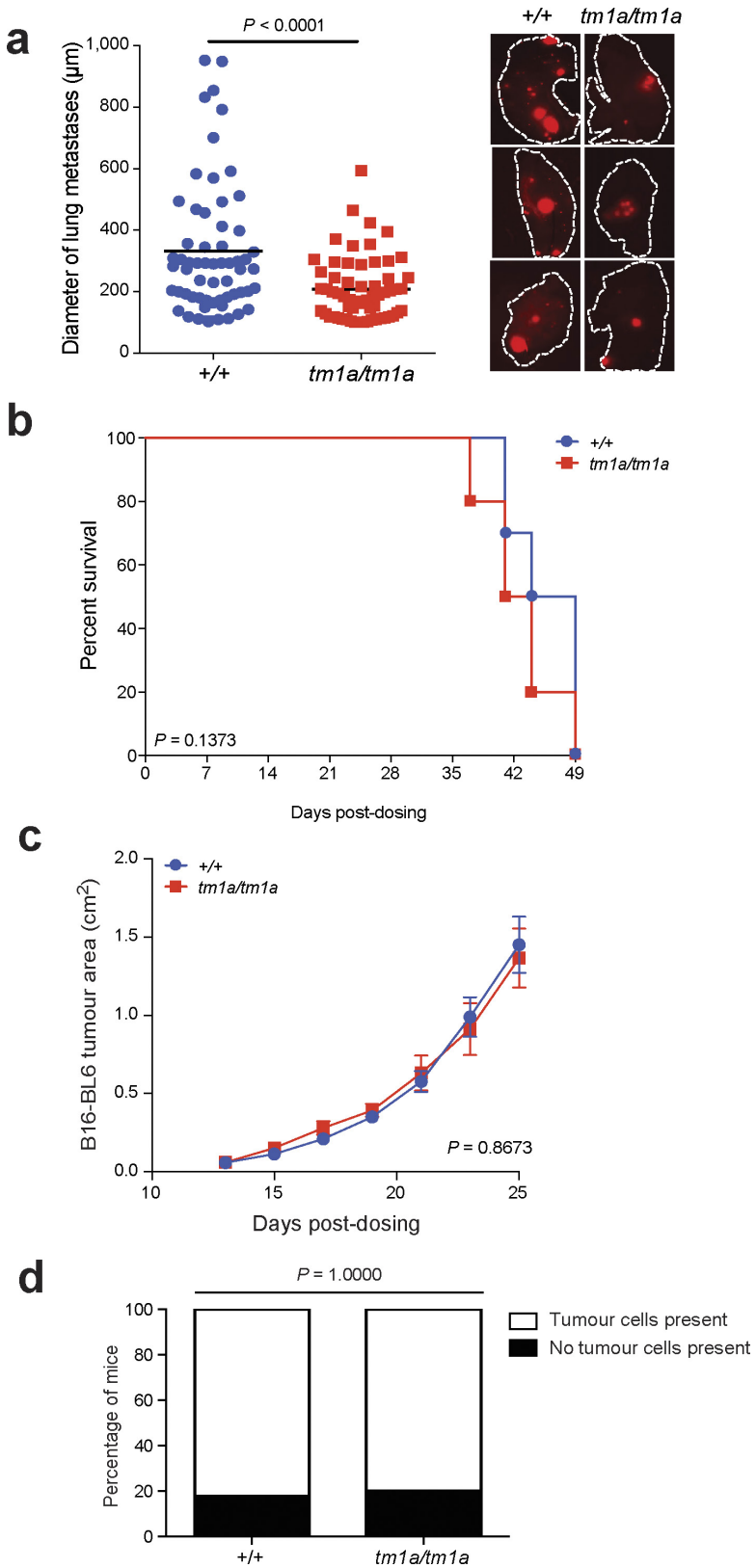

Extended Data Figure 2 | Spontaneous pulmonary metastases and primary tumour growth in *Spns2* mice. a, Size measurements of spontaneous pulmonary HCmel12–mCherry melanoma cell metastases of male mice with representative fluorescent images (lines indicate the edge of the lungs); $n = 10$ per genotype, horizontal bars represent mean (of 50 individual metastases counted per genotype) (one-way ANOVA with blocking factor of experiment, cumulative results of two independent experiments shown). **b**, Survival curve of +/+ and *tm1a/tm1a* male mice ($n = 10$ per genotype) in a spontaneous metastasis assay using HCmel12–mCherry cells (log-rank test (Mantel–Cox), cumulative results of two independent experiments shown). **c**, Growth of subcutaneously administered B16-BL6 cells in +/+ (four male, five female) and *tm1a/tm1a* (five male, one female) mice. Symbols represent mean ± s.e.m. with a two-tailed unpaired *t*-test with Welch's correction used to compare the area under the curve. **d**, Incidence of cancer in aged (>40 weeks) +/+ ($n = 15$; 4 males, 11 females) and *tm1a/tm1a* ($n = 18$; 5 males, 13 females) mice. Statistical analysis was performed using a Fisher's exact test.

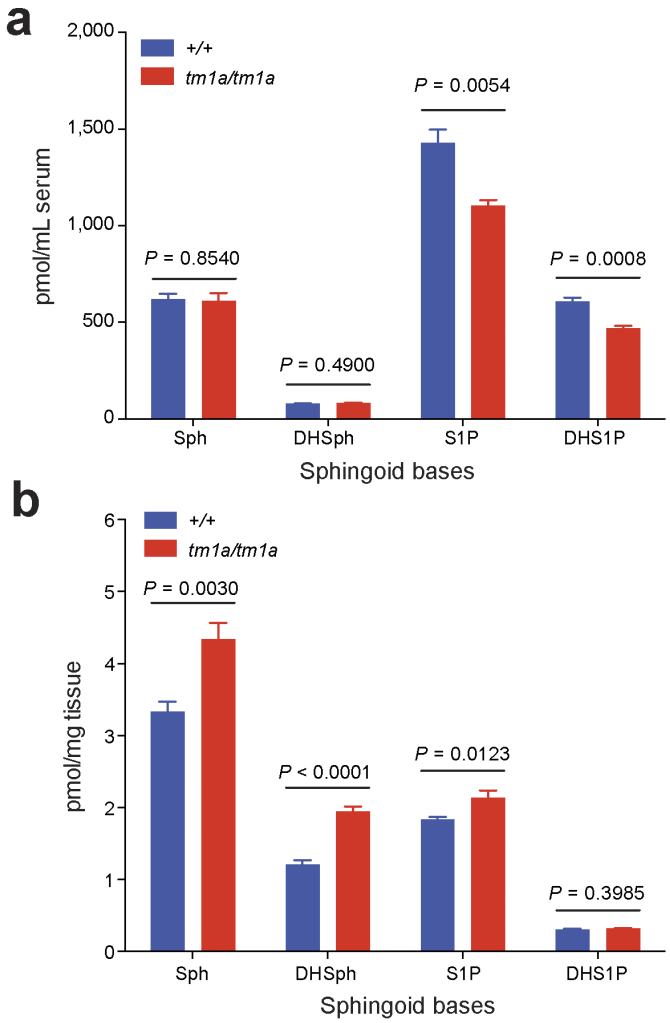

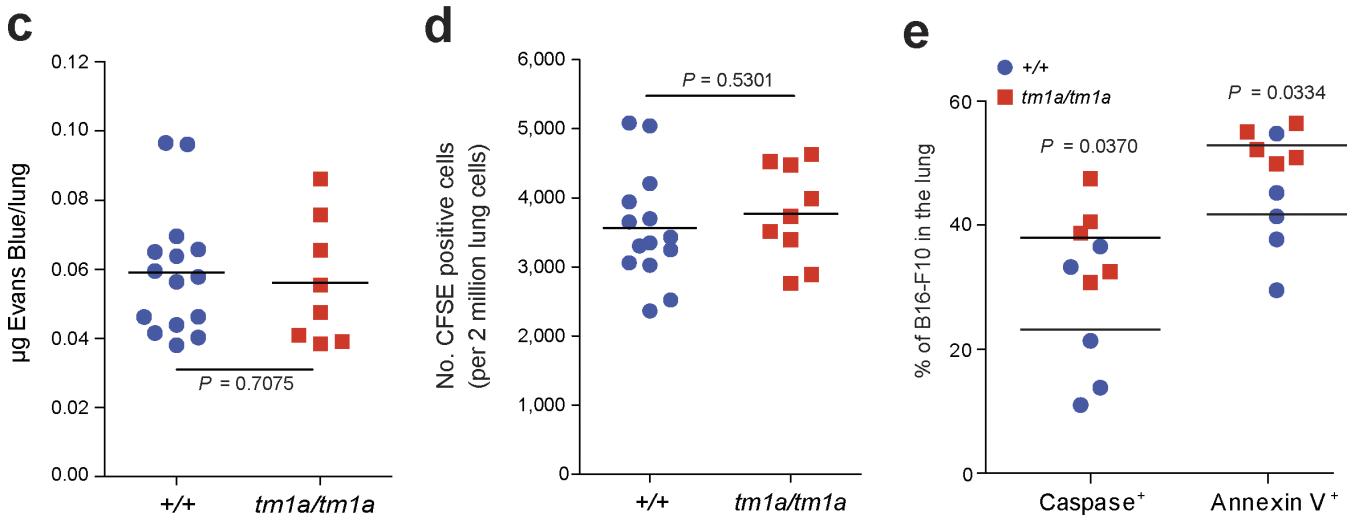

Extended Data Figure 3 | Phenotyping of the serum and lungs of *Spns2* mice. Sphingoid base levels in the (**a**) serum (+/+, $n = 5$; *tm1a/tm1a*, $n = 4$) and (**b**) lungs (+/+, $n = 6$; *tm1a/tm1a*, $n = 5$) of male mice; data are mean ± s.e.m., multiple two-tailed unpaired *t*-tests with *P* value adjusted by the Holm–Šídák method with α set to 5%. Sph, sphingosine; DHSph, dihydrosphingosine; S1P, sphingosine-1-phosphate; DHS1P, dihydrosphingosine-1-phosphate. **c**, Micrograms of extravasated Evans blue dye in the lungs of +/+ and *tm1a/tm1a* male mice. **d**, Number of CFSE-labelled B16-F10 cells present in the lungs of female mice 90 min after administration. **e**, Levels of apoptosis in B16-F10–mCherry cells 12 h after administration to male mice. Shown are representative data from three independent experiments, with symbols representing individual mice. *P* values are indicated from two-tailed unpaired *t*-test with Welch's correction (**c**–**e**).

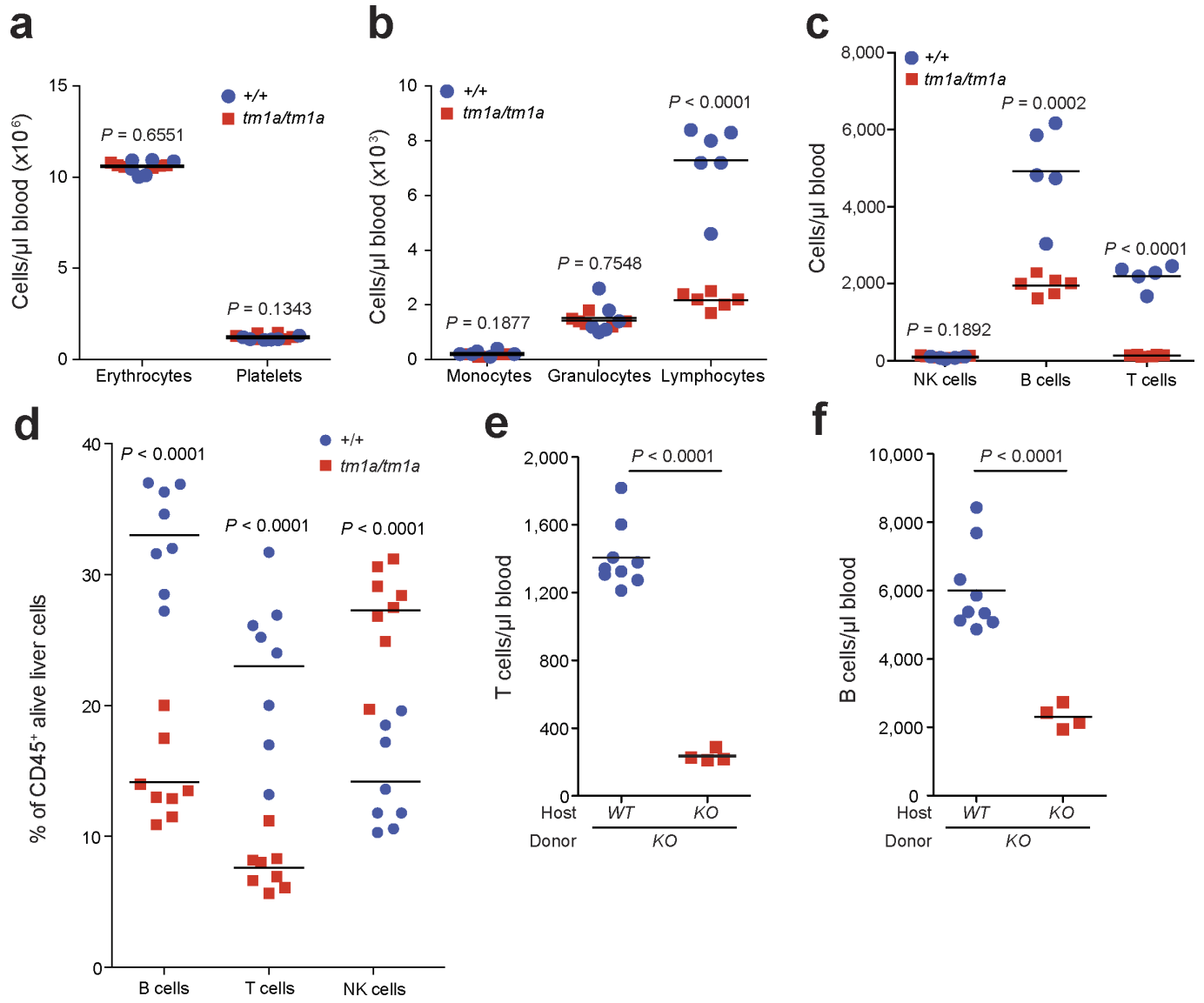

Extended Data Figure 4 | Phenotypic characterization of the haematopoietic system of *Spns2* mice. a–c, The numbers of erythrocytes and platelets, monocytes, granulocytes and lymphocyte subsets present in the blood of naive +/+ and *tm1a/tm1a* female mice (multiple two-tailed unpaired *t*-tests with *P* value adjusted by the Holm–Šídák method with α set to 5%; data shown are representative of three independent experiments). **d**, Analysis of lymphocyte subsets in the liver of naive +/+ and *tm1a/tm1a* female mice (multiple two-tailed unpaired *t*-tests with *P* value adjusted by the Holm–Šídák method with α set to 5%; data shown are representative of three independent experiments). **e**, **f**, T- and B-lymphocyte numbers in the blood of male naive (unstimulated) bone marrow chimaeras (unpaired two-tailed *t*-test with Welch's correction; data shown are representative of two independent experiments). Symbols represent individual mice; horizontal bars represent mean.

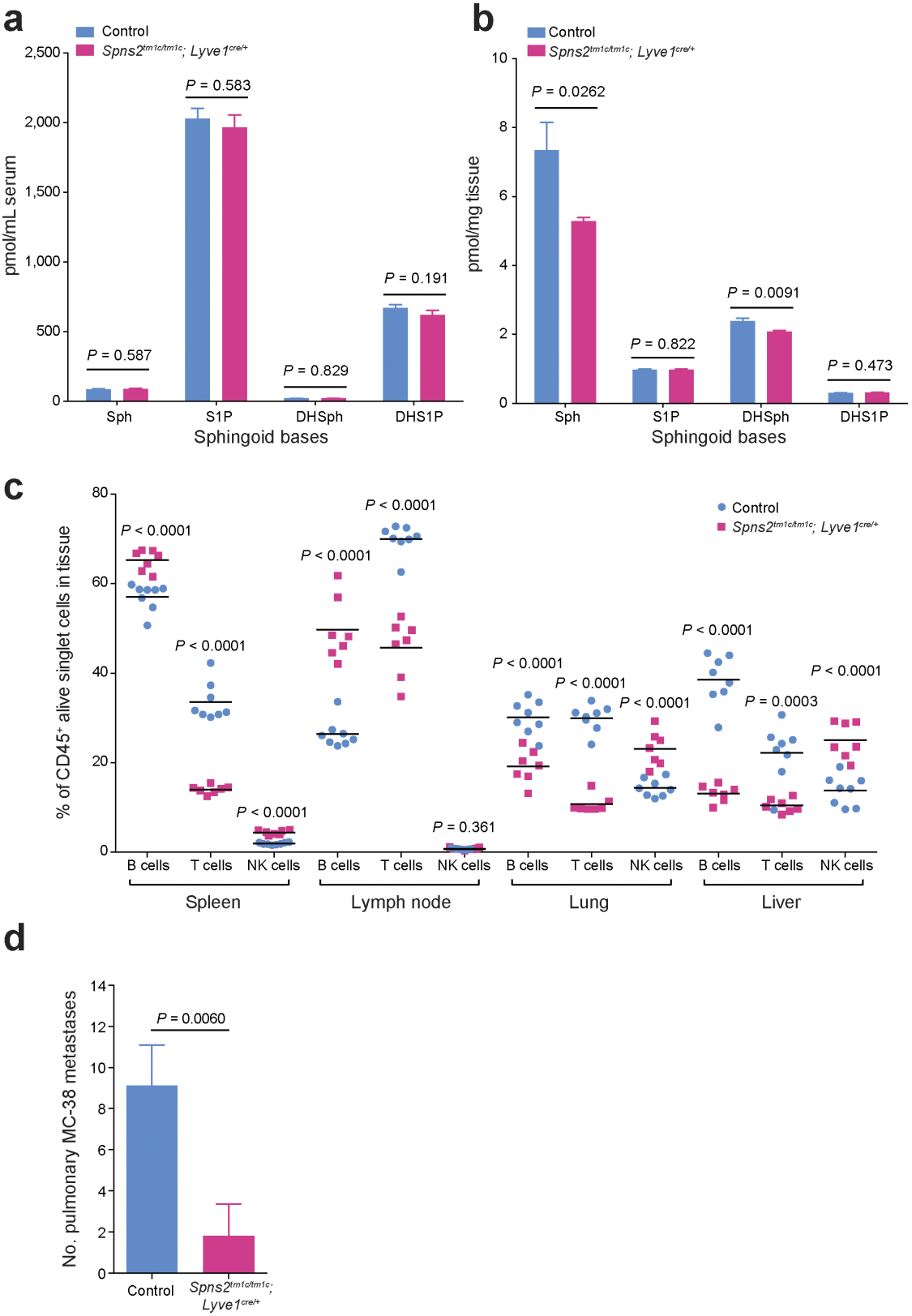

Extended Data Figure 5 | Characterization of the phenotype of lymphatic endothelial cell *Spns2* deficient mice. a, **b**, Sphingoid base levels in the (**a**) serum or (**b**) lung of control and *Spns2*$^{tm1c/tm1c}$; *Lyve1*$^{cre/+}$ male mice (data are mean ± s.e.m., control $n = 11$, *Spns2*$^{tm1c/tm1c}$; *Lyve1*$^{cre/+}$ $n = 10$, multiple two-tailed unpaired *t*-tests with *P* value adjusted by the Holm–Šídák method with α set to 5%). Sph, sphingosine; DH-Sph, dihydrosphingosine; S1P, sphingosine-1-phosphate; DH-S1P, dihydrosphingosine-1-phosphate. **c**, Lymphocyte subsets in the spleen, lymph node, lung and liver of +/+ and *tm1a/tm1a* male mice (symbols represent individual mice, horizontal bars represent mean, multiple two-tailed unpaired *t*-tests with *P* value adjusted by the Holm–Šídák method with α set to 5%; data shown are representative of three independent experiments). **d**, Experimental metastasis assay using MC-38 cells in control ($n = 9$) and *Spns2*$^{tm1c/tm1c}$; *Lyve1*$^{cre/+}$ ($n = 5$) in female mice. Data shown are mean ± s.e.m., Mann–Whitney test, representative of three independent experiments.

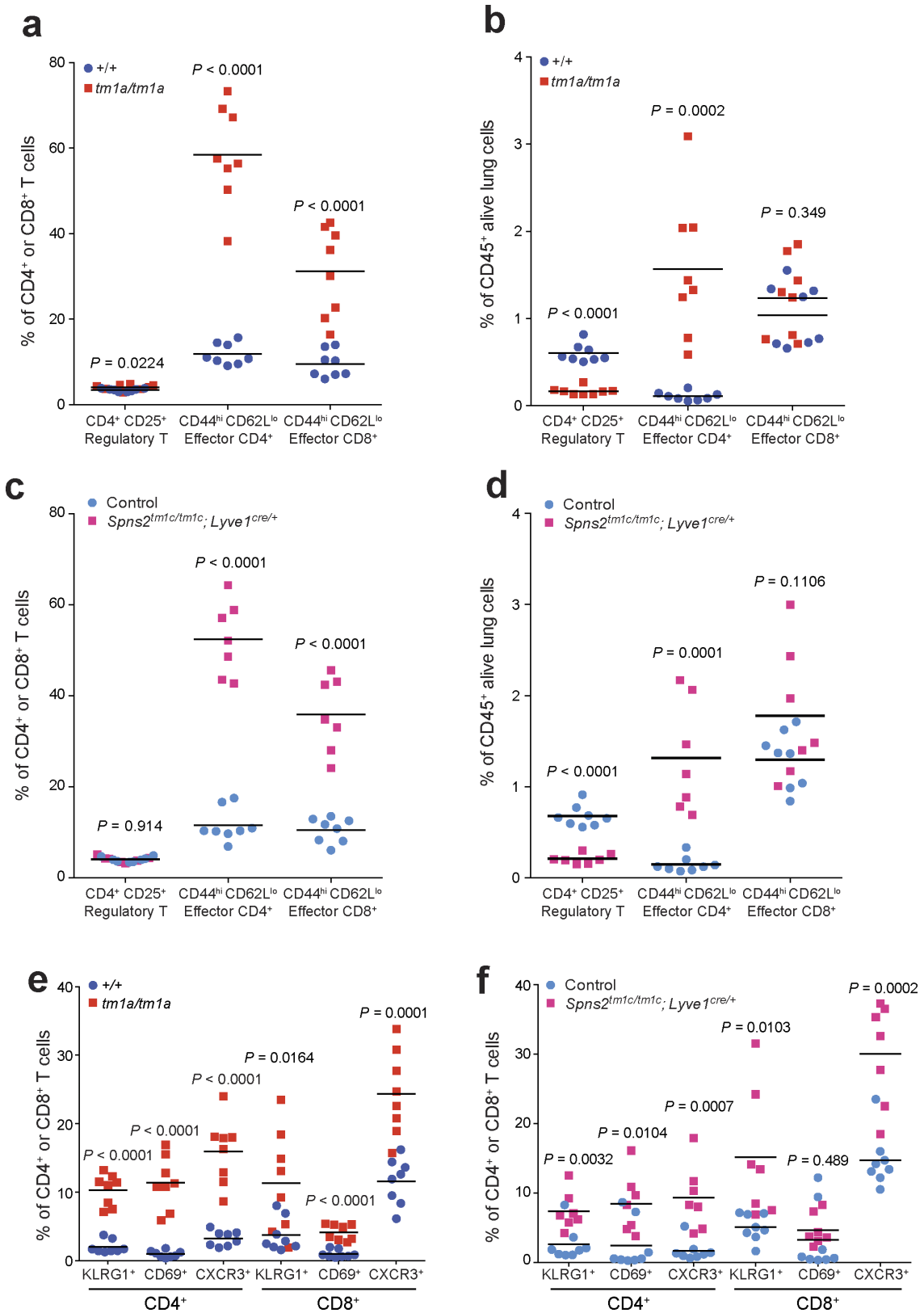

Extended Data Figure 6 | T cell subsets in the lungs of *Spns2* mice. The proportion of T cell subsets present in the lungs of naive +/+ and *tm1a/tm1a* female mice (**a**, **b**, **e**) and control and *Spns2*$^{tm1c/tm1c}$; *Lyve1*$^{cre/+}$ male mice (**c**, **d**, **f**). Data are shown as percentage of parent CD4$^+$ and CD8$^+$ T cells (**a**, **c**, **e**, **f**) or percentage of CD45$^+$ alive lung cells present (**b**, **d**). Symbols represent individual mice with horizontal bar at the mean. *P* values are indicated from two-tailed unpaired *t*-test adjusted by the Holm–Šídák method with α set to 5%. Data shown are representative of three independent experiments.

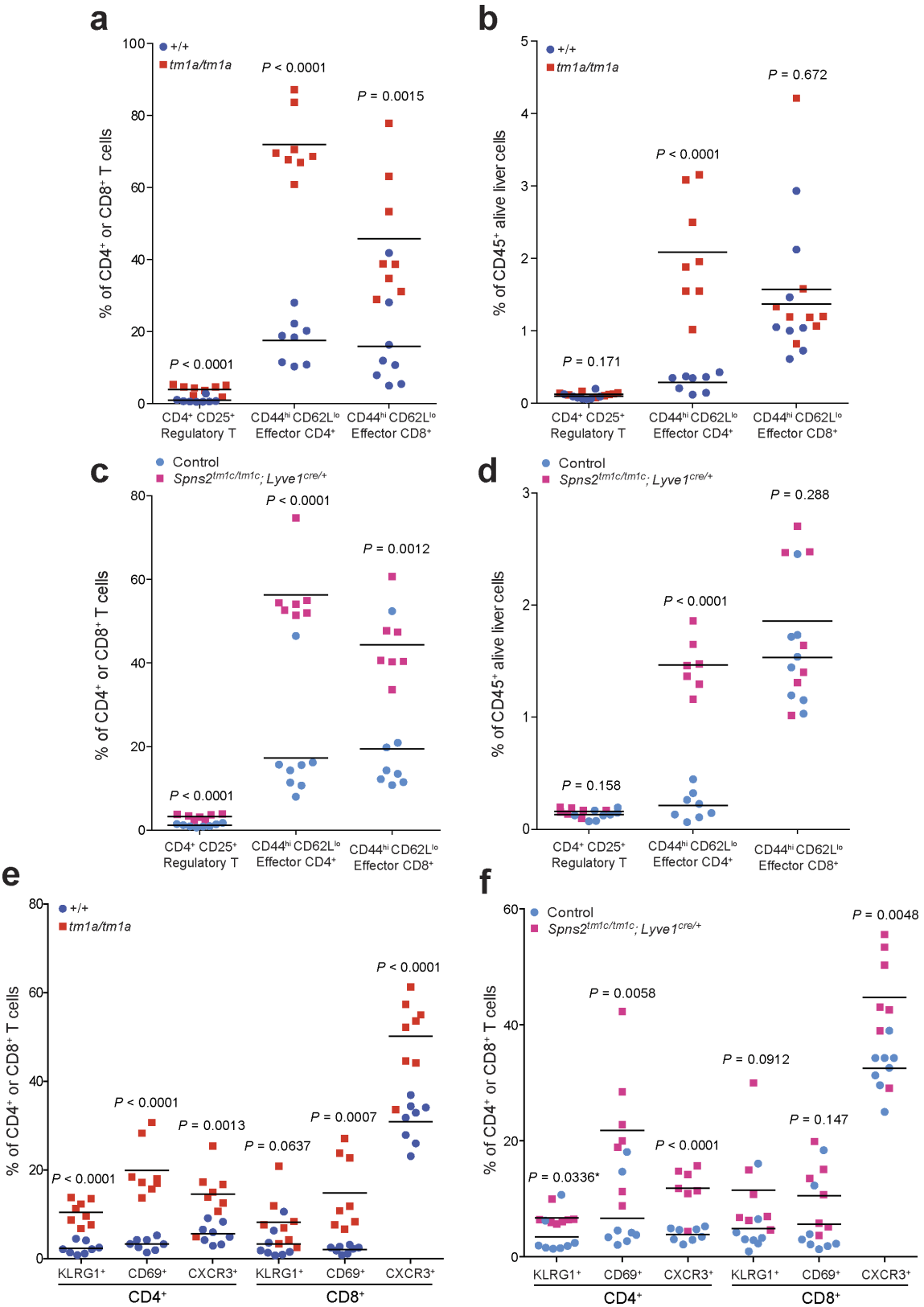

Extended Data Figure 7 | T cell subsets in the liver of *Spns2* mice. The proportion of T cell subsets present in the liver of naive +/+ versus *tm1a/tm1a* female mice and control versus *Spns2*$^{tm1c/tm1c}$; *Lyve1*$^{cre/+}$ male mice. Data are shown as percentage of parent CD4$^+$ and CD8$^+$ T cells (**a**, **c**, **e**, **f**) or percentage of CD45$^+$ alive liver cells present (**b**, **d**). Symbols represent individual mice; statistical analysis used multiple two-tailed unpaired *t*-tests with *P* value adjusted by the Holm–Šídák method with α set to 5%, with * indicating a *P* value not considered significant after correcting for multiple testing. Data shown are representative of three independent experiments.

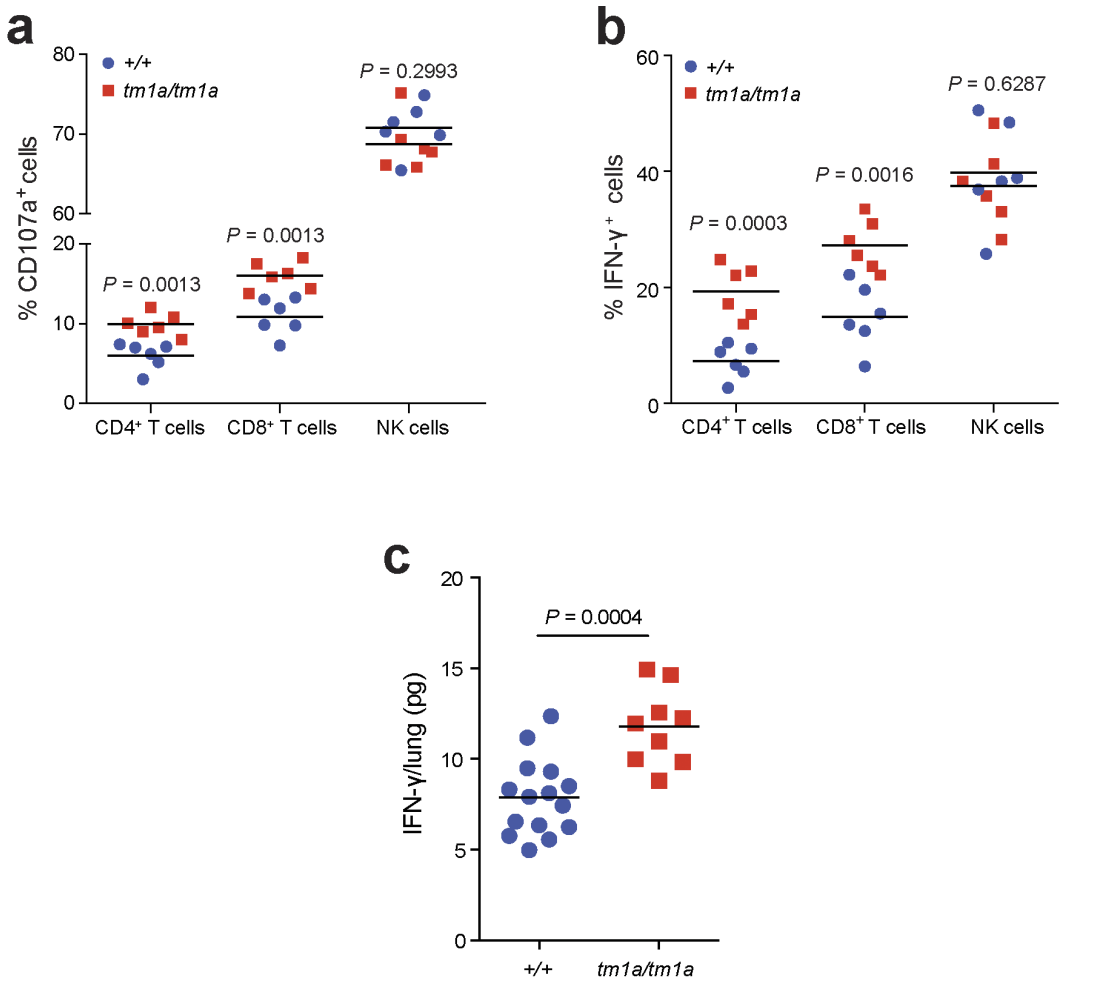

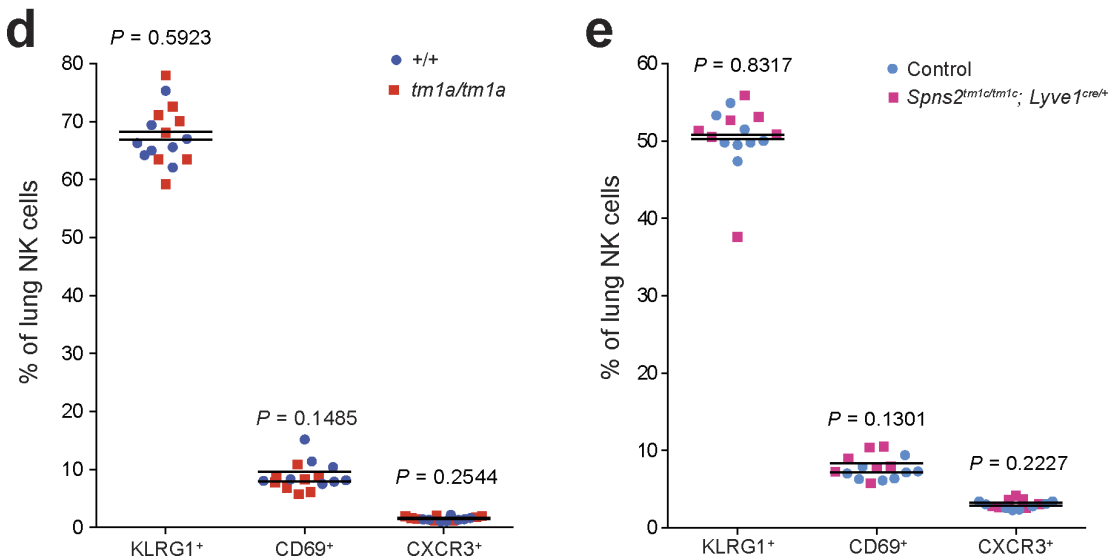

Extended Data Figure 8 | Phenotyping of *Spns2* lungs. a, **b**, *Ex vivo* re-stimulation (PMA/ionomycin) of pulmonary leukocytes from B16-F10-stimulated +/+ and *tm1a/tm1a* female mice (two-tailed unpaired *t*-test adjusted by the Holm–Šídák method with α set to 5%). **c**, Measurement of IFN-γ in lungs of MC-38-stimulated +/+ and *tm1a/tm1a* male mice (two-tailed unpaired *t*-test with Welch's correction). **d**, **e**, The proportion of NK cell subsets present in the lungs of naive +/+ versus *tm1a/tm1a* female mice (**d**) and control versus *Spns2*$^{tm1c/tm1c}$; *Lyve1*$^{cre/+}$ male mice (**e**) (multiple two-tailed unpaired *t*-tests with *P* value adjusted by the Holm–Šídák method with α set to 5%). Symbols represent individual mice, horizontal bars represent mean; data shown are representative of three independent experiments.

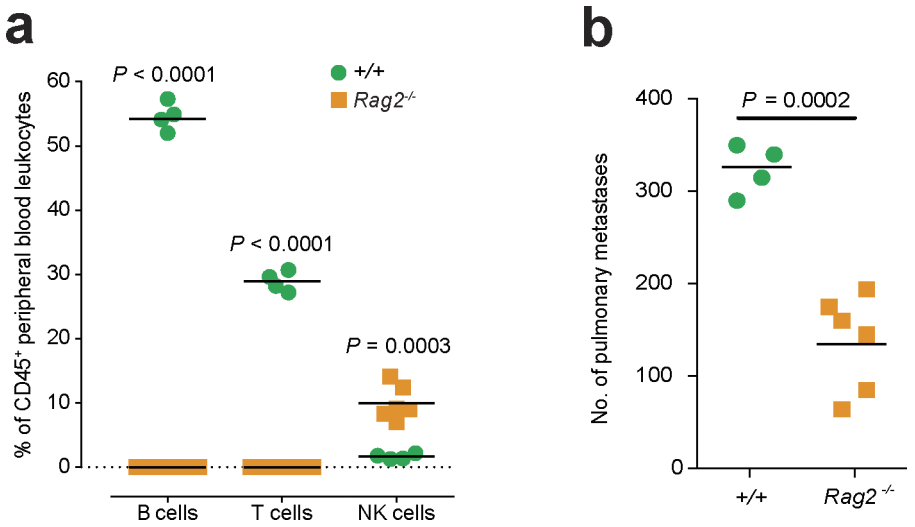

Extended Data Figure 9 | Studies in T- and B-cell-deficient mice. **a**, Measurement of lymphocyte subsets in the blood of +/+ and *Rag2*$^{-/-}$ mice (multiple two-tailed unpaired *t*-tests with *P* value adjusted by the Holm–Šídák method with α set to 5%). **b**, Experimental metastasis assay using B16-F10 cells in +/+ and *Rag2*$^{-/-}$ female mice (Mann–Whitney test). Symbols represent individual mice, horizontal bars represent mean; data shown are representative of three independent experiments.

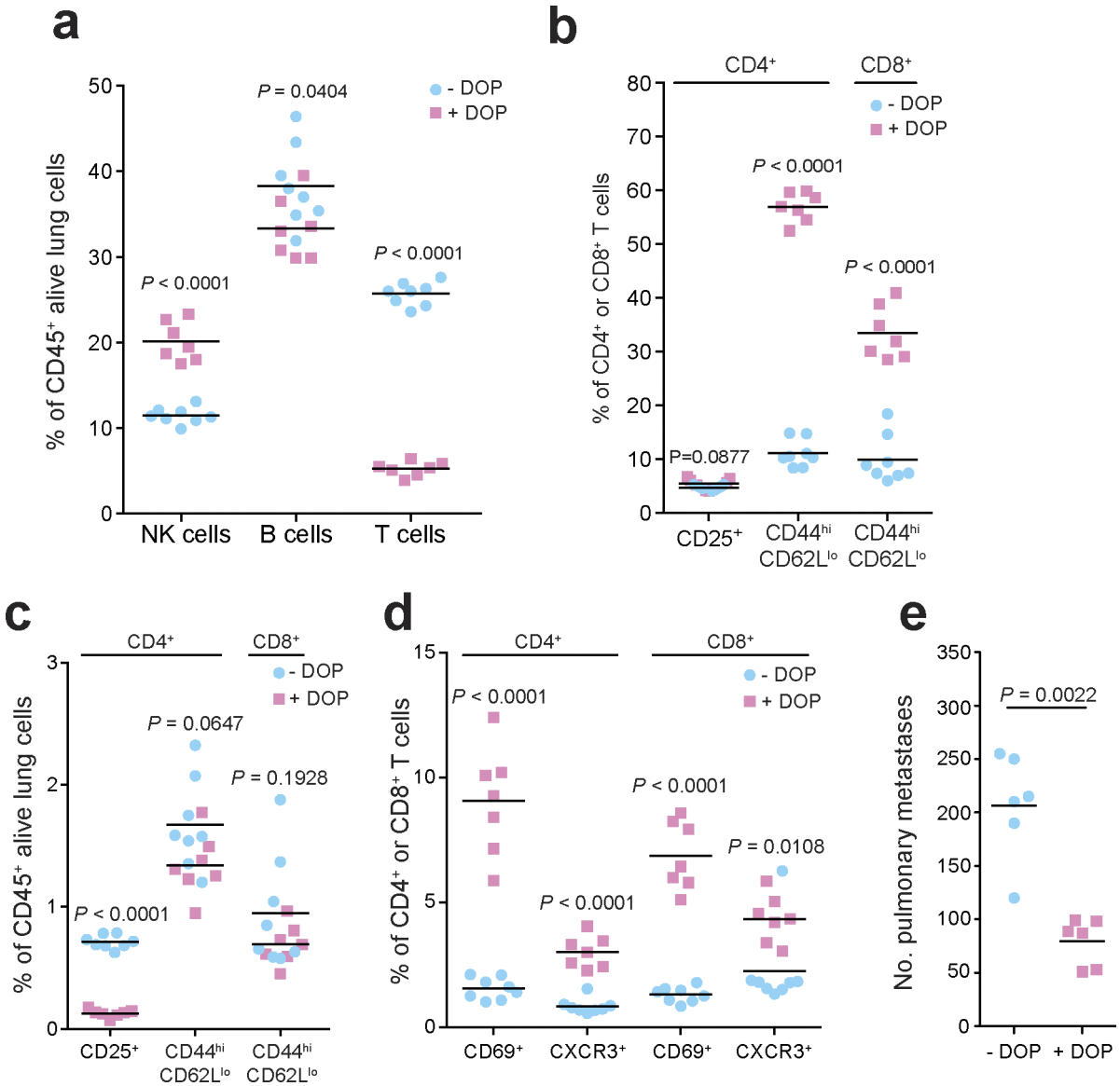

Extended Data Figure 10 | Characterization of the leukocyte composition and phenotype in DOP-treated mice. a–d, The number of leukocytes and T cell subsets present in the lungs of B16-F10-dosed glucose- or DOP-treated wild-type male mice presented as the percentages of viable $CD45^+$ lung leukocytes (**a**, **c**) or parent $CD4^+$ or $CD8^+$ T cells (**b**, **d**) (multiple unpaired *t*-tests with *P* value adjusted by the Holm–Šídák method with α set to 5%). **e**, Experimental metastasis assay in B16-F10 dosed glucose- or DOP-treated wild-type female mice (Mann–Whitney test). Symbols represent individual mice, horizontal bars represent mean; data shown are representative of two independent experiments.

Manuscript Details

Manuscript number	JBIOR_2017_56
Title	SPHINGOSINE KINASE 1 IN BREAST CANCER
Article type	Review Article
Keywords	sphingosine-1-phosphate, sphingosine kinase, estradiol, breast cancer, FTY720/fingolimod
Corresponding Author	SARAH Spiegel
Corresponding Author's Institution	VCU
Order of Authors	SARAH Spiegel, Kurt Geffken

Submission Files Included in this PDF

File Name [File Type]

Sphingosine Kinase 1 in Breast Cancer REV FINAL.docx [Manuscript File]

Figure 1.pdf [Figure]

Conflict of interest form.docx [Conflict of Interest]

To view all the submission files, including those not included in the PDF, click on the manuscript title on your EVISE Homepage, then click 'Download zip file'.

SPHINGOSINE KINASE 1 IN BREAST CANCER

Kurt Geffken and Sarah Spiegel

Department of Biochemistry and Molecular Biology and the Massey Cancer Center

Virginia Commonwealth University School of Medicine

Richmond, Virginia 23298 USA

*Corresponding Author: Tel.: +1-804-828-9330, E-mail: sarah.spiegel@vcuhealth.org

ABSTRACT

Breast cancer affects 1 out of 8 women in the US and is the second highest cause of death from cancer for women, leading to considerable research examining the causes, progression, and treatment of breast cancer. Over the last two decades, sphingosine-1-phosphate (S1P), a potent sphingolipid metabolite, has been implicated in many processes important for breast cancer including growth, progression, transformation and metastasis, and is the focus of this review. In particular, one of the kinases that produces S1P, sphingosine kinase 1 (SphK1), has come under increasing scrutiny as it is commonly upregulated in breast cancer cells and has been linked with poorer prognosis and progression, possibly leading to resistance to certain anti-cancer therapies. In this review, we will also discuss preclinical studies of both estrogen receptor (ER) positive as well as triple-negative breast cancer mouse models with inhibitors of SphK1 and other compounds that target the S1P axis and have shown good promise in reducing tumor growth and metastasis. It is hoped that in the future this will lead to development of novel combination approaches for effective treatment of both conventional hormonal therapy-resistant breast cancer and triple-negative breast cancer.

Keywords: sphingosine-1-phosphate, sphingosine kinase, estradiol, breast cancer, FTY720/fingolimod.

Abbreviations: BCSCs, breast cancer stem cells; ,ER, estrogen receptor; EGFR, epidermal growth factor receptor; ERK, extracellular signal regulated kinase; E2, 17β-estradiol; HDAC, histone deacetylase; HER2, human epidermal growth factor receptor 2; MAPK, mitogen activated protein kinase; PKC, protein kinase C; RTK, receptor

tyrosine kinase; SphK, sphingosine kinase; S1P, sphingosine-1-phosphate; S1PR, S1P receptor; TNBC, triple-negative breast cancer;

INTRODUCTION

Breast cancer affects nearly 1 out of every 8 women over their lifetime and is the second leading cancer cause of death for women behind lung cancer in the US. Fortunately, over the last 30 years, breast cancer death rates have been dropping due to increased awareness of the disease, advances in detection, and better treatments. A large factor in these better treatments has been development of hormonal therapies to directly target specific receptors in the cancer cells such as estrogen (ER) and progesterone receptors (PR) that are present in roughly 70% of breast cancers. ER positive tumors in particular can be treated with estrogen antagonists such as tamoxifen to great effect with less side effects than traditional chemotherapy. The human epidermal growth factor receptor 2 (HER2), that is upregulated in 10 to 15% of breast cancers tumors and can also be treated with a monoclonal antibody. However, there are still 15 to 20% of tumors that are ER/PR/HER2 negative, termed triple negative breast cancer (TNBC), which are usually more aggressive and metastatic with significantly worse prognosis. Therefore, current cancer research is also focused on deeper understanding of novel signaling pathways that can contribute to breast cancer growth and metastasis. In the last 20 years, it has become apparent that the bioactive sphingolipid metabolite, sphingosine-1-phosphate (S1P), regulates processes important for breast cancer including inflammation that can drive tumorigenesis including angiogenesis, which provides cancer cells with nutrients and oxygen, cell growth and survival, as well as migration and invasion important for metastasis (Maczis et al., 2016; Newton et al., 2015; Pyne and Pyne, 2010). In this review, we will summarize current research findings on S1P in breast cancer and examine the roles of the

S1P/sphingosine kinase 1 (SphK1) axis in breast cancer signaling, prognosis, progression and as a possible target for future treatments, especially for TNBC and tumors that show resistance to typical first line treatments.

FORMATION OF SPHINGOSINE-1-PHOSPHATE

Sphingolipids are important membrane constituents of all eukaryotic cells that also generate bioactive metabolites, such as S1P. The formation of S1P from sphingosine, produced by degradation of sphingolipids, begins with the activation of one of two enzymes, SphK1 or SphK2, resulting in the former case in its translocation from the cytosolic compartment to the plasma membrane where its substrate sphingosine resides (Hannun and Obeid, 2008). Numerous growth factors such as EGF, hormones, such as estradiol (E2), and pro-inflammatory cytokines such as IL-1 and IL-6 activate SphK1 (Gao et al., 2015; Maceyka et al., 2012; Maceyka and Spiegel, 2014; Maczis et al., 2016). In many cases, it has been shown that this is due to stimulation of extracellular signal-regulated kinases 1/2 (ERK1/2) that in turn phosphorylates SphK1 on Ser225 allowing for its specific targeting to the plasma membrane (Pitson et al., 2003). This is in contrast to SphK2 that also resides in intracellular compartments, including the nucleus, and produces S1P there (Hait et al., 2009). As with other potent mediators, S1P is rapidly turned over either by dephosphorylation back to sphingosine by phosphatases or irreversibly cleaved by S1P lyase to ethanolamine phosphate and hexadecenal (Hannun and Obeid, 2008; Maceyka and Spiegel, 2014).

SPHINGOSINE-1-PHOSPHATE SIGNALING IN BREAST CANCER

Following activation of SphK1 and restricted formation of S1P, the majority of the effects mediated by S1P occur after its export from the cell by the specific transporter

called spinster 2 (Spns2) or by ATP-binding cassette transporters ABCA1, ABCC1, and ABCG2. S1P then can bind to one of five specific G protein-coupled cell surface S1P receptors (S1PR1-5) in an autocrine/paracrine manner, termed “inside-out” signaling. This leads to stimulation of downstream signaling mediated by overlapping G-proteins (Maceyka et al., 2012; Maczis et al., 2016; Takabe et al., 2008) (Fig. 1). A complete description of all of the interconnected signaling pathways that are activated by S1P is beyond the scope of this review, and this area has been extensively reviewed (Kihara et al., 2014). Therefore, we will mainly focus on S1PR1 and S1PR3, two receptors that have been linked to breast cancer progression.

Intriguingly, S1PR1 has been linked to persistent activation of signal transducer and activator of transcription 3 (STAT3). STAT3 has been shown to be involved in many aspects of tumor growth and metastasis by activating a wide range of pathways promoting proliferation, survival, inflammation, invasion, and angiogenesis (Yu et al., 2014). STAT3 also enhances transcription of S1PR1 and activation of S1PR1 by S1P reciprocally activates STAT3 (Alshaker et al., 2014; Alshaker et al., 2015; Lee et al., 2010; Liang et al., 2013). In breast cancer in particular, persistent STAT3 activation seems to be mainly due to upregulation of the pro-inflammatory cytokine IL-6 and S1PR1 (Alshaker et al., 2014; Alshaker et al., 2015; Lee et al., 2010). Moreover, IL-6 can activate SphK1 leading to a strong feed-forward mechanism promoting cancer cell progression (Lee et al., 2010). This signaling pathway is further complicated in ER negative breast cancer cells. as the adipokine leptin, a product of adipocytes, has also been shown to upregulate STAT3 and SphK1. SphK1 in turn induces production of IL-6, which then activates STAT3 (Alshaker et al., 2014; Alshaker et al., 2015).

Pharmacological and molecular approaches further demonstrated that leptin-induced SphK1 activity and expression are mediated by activation of ERK1/2 and Src family kinase pathways, but not by the major pathways downstream of the leptin receptor, janus kinase 2 (JAK2) (Alshaker et al., 2015). As obesity is a risk factor for breast cancer and related to poorer prognosis, these studies could have implications for ER-negative breast cancer.

Binding of S1P to S1PR1 has also been shown to activate various receptor tyrosine kinases (RTKs) important for angiogenesis and proliferation such as VEGFR, EGFR, and PDGFR. This can result in “criss-cross” pathway activations as the growth factors that activate these RTKs can also activate SphK1. For example, EGF activation of SphK1 plays an important role in the migration of breast cancer cells towards EGF along with increased cell growth (Sarkar et al., 2005). S1P also potentiates the EGFR signaling pathway by insulin-like growth factor binding protein 3 (IGFBP-3), a growth promoter associated with poorer prognosis, suggesting that inhibition of both EGFR and SphK1 could have beneficial therapeutic effects in TNBC (Martin et al., 2014). Moreover, VEGF-mediated activation of SphK1 plays an essential role in regulating angiogenesis and lymphangiogenesis (Anelli et al., 2010; Nagahashi et al., 2012).

As for S1PR3, its activation via S1P was linked to the activation of the Notch signaling pathway along with p38MAPK in breast cancer stem cells (BCSCs) leading to proliferation and tumorigenicity (Hirata et al., 2014). BCSCs can also be activated by carcinogens, such as benzyl butyl phthalate, which has been shown to increase SphK1 expression leading to S1PR3 activation, implying that S1PR3 is a determinant of pollutant-driven breast cancer metastasis (Wang et al., 2016).

Most of S1PR3's cancer promoting and pro-survival effects can be attributed to sustained activation of ERK1/2 and AKT/PI3K pathways, key regulators of cell cycle progression, survival, and proliferation mechanisms in breast cancer cells (Datta et al., 2014; Wang et al., 2016; Watson et al., 2010). In triple-negative MDA-MB-231 breast cancer cells, early and sustained phosphorylation of both ERK1/2 and AKT/PI3K was inhibited by a SphK1 inhibitor while only sustained activation was inhibited by pertussis toxin, a potent G protein inhibitor, suggesting that S1PRs are crucial only for sustained activation (Datta et al., 2014). Aside from activating its own downstream signaling cascade, the AKT/PI3K pathway is involved in crosstalk with several other pathways, including RAS/RAF/MEK and ER, further strengthening the interconnecting pro-survival and progression pathways (Maiti et al., 2017). Another study in TNBC cells substantiated a link between sphingosine, SphK1, and the protein kinase C (PKC) serine/threonine kinase family, important regulators of cell proliferation and survival (Kotelevets et al., 2012). This study also showed that targeting SphK1 in triple-negative MDA-MB-231 breast cancer cells decreased proliferation and survival by compromising PKC activity and cytokinesis (Kotelevets et al., 2012). While the exact mechanisms of these pathways have not been elucidated, they support the significance of SphK1 as a target for cancer therapy. A recent study with MDA-MB-231 cells looked at how S1P signaling affected adhesion and invasion via the tumor cell microenvironment. It was reported that extracellular matrix rigidity-dependent S1P secretion regulates metastatic cancer cell invasion and adhesion (Ko et al., 2016). These results suggest that alterations in the mechanical environment of the extracellular matrix surrounding the tumor cells actively regulate secretion of S1P, which in turn, may contribute to cancer

progression. In summary, many of the pathways modulated by the SphK1/S1P/S1PR axis in breast cancer cells are overlapping, promoting their growth, survival, proliferation, and metastasis (Fig. 1).

In addition to the very well-known functions of S1P as a ligand for S1PRs, recent studies suggest that S1P also has important intracellular actions (Maceyka et al., 2012). Especially relevant is the observation that SphK2 is present in the nucleus of many breast cancer cell lines (Hait et al., 2009; Igarashi et al., 2003; Sankala et al., 2007) where it produces S1P that inhibits class I histone deacetylases (HDACs) (Hait et al., 2009). Thus, it was suggested that HDACs are direct intracellular targets of S1P and link nuclear sphingolipid metabolism and S1P to epigenetic regulation of expression of specific genes (Hait et al., 2009). Recently, we found that FTY720 is also phosphorylated in breast cancer cells by nuclear SphK2 and accumulates there. Moreover, like S1P, nuclear FTY720-P is also a potent inhibitor of class I HDACs. Furthermore, we observed that high fat diet increased triple-negative spontaneous breast tumors and HDAC activity in MMTV-PyMT transgenic mice that was suppressed by oral administration of FTY720. Interestingly, this treatment not only inhibited HDACs, it also reversed high fat diet-induced loss of ER and PR in advanced carcinoma (Hait et al., 2015). Furthermore, treatment with FTY720 also re-expressed ER and increased therapeutic sensitivity of TNBC syngeneic breast tumors to tamoxifen in vivo more potently than a known HDAC inhibitor. This work suggests that in combination, FTY720 could be an effective treatment of both conventional hormonal therapy-resistant breast cancer and triple-negative breast cancer (Hait et al., 2015).

SPHINGOSINE KINASE 1 AND ESTROGEN RECEPTOR SIGNALING

Nearly 80% of breast cancers are ER positive, meaning they are dependent on estrogens such as 17β-estradiol (E2) to signal growth, proliferation and metastasis. E2 normally binds to ER in the cytoplasm and after dimerization, translocates to the nucleus. In the nucleus, the ER dimers bind to estrogen response elements and act as transcription factors to activate or repress gene transcription (Klinge, 2001). E2 can also induce rapid, non-genomic cellular changes through membrane ERs that are still ill defined, including the splice variant ER36 and the G protein-coupled receptor GPR30 (Wang and Yin, 2015; Zhou et al., 2016). These membrane ERs have been shown to activate SphK1, producing S1P and activate signaling pathways downstream of S1PRs leading to increased cell growth, higher microvessel density in tumors, and enhanced resistance to anti-cancer drugs in response to hormonal therapies (Maczis et al., 2016; Sukocheva et al., 2006; Sukocheva et al., 2013; Takabe et al., 2010). GPR30 was suggested to activate SphK1 as its downregulation by anti-sense oligonucleotides inhibited E2-mediated activation of SphK1 in MCF-7 breast cancer cells (Sukocheva et al., 2006). However, the identity of the responsible receptor has not yet been conclusively established. E2-mediated formation of S1P led to rapid release of S1P from breast cancer cells via the ABCC1 and the ABCG2 transporters (Takabe et al., 2010) and “inside out” signaling by S1P (Maczis et al., 2016; Sukocheva et al., 2006; Sukocheva et al., 2013). Furthermore, inhibiting these transporters blocked E2-induced activation of ERK1/2 (Takabe et al., 2010). It was convincingly demonstrated that activation of S1PR3 by S1P transactivated EGFR through a pathway mediated by Src and matrix metalloproteases. This switch from E2/ER-mediated growth to SphK1/EGFR activation has also been thought to contribute to resistance to hormonal therapies such

as tamoxifen (Maczis et al., 2016; Sukocheva and Wadham, 2014; Sukocheva et al., 2006).

SphK1 activity has also been linked to the effects of several microRNAs that are regulated by ER. miR-515-5P, a tumor suppresser, was shown to reduce SphK1 activity and loss of miR-515-5P resulted in increased oncogenic SphK1 activity. In addition, E2 treatment downregulated miR-515-5P levels, and miR-515-5p is downregulated in ER-positive compared to ER-negative breast cancers (Pinho et al., 2013).

SPHINGOSINE KINASE 1 AND BREAST CANCER PROGNOSIS

Over the last few years, new evidence from several studies has illuminated the multi-factorial role of the SphK1/S1P axis in breast cancer and its link with worse prognosis and overall outcomes (Ruckhaberle et al., 2008). It also usually corresponds with upregulation of associated S1PRs and chemotherapeutic resistance (Gao et al., 2015). In one study, 62.5% of tumors analyzed (20 out of 32) had at least a 2-fold increase in SphK1 mRNA expression compared to surrounding normal breast tissue (Datta et al., 2014). Furthermore, ER negative tumors had higher SphK1 levels than ER-positive tumors and the deadlier, triple-negative tumors had the highest levels of SphK1 expression of all tumor types examined. Overall, the analysis revealed an inverse correlation between SphK1 levels and survival of breast cancer patients. One of the possible causes investigated in this study was resistance to doxorubicin and docetaxel-based chemotherapies, mainstays for treatment of ER positive breast cancer, and it was found that non-responders to treatment had significantly higher SphK1 mRNA levels. This infers that SphK1 does not just promote progression and growth of tumors but also impacts survival through its effects on drug resistance (Datta et al.,

2014). Patients with high levels of cytoplasmic Sphk1 compared to low SphK1 had a nearly 8-years shorter mean time to recurrence on tamoxifen (12.61 years with low SphK1 and 4.65 years with high SphK1 expression). Further investigations examined expression of S1PR1 and S1PR3 in particular and it was noted that patients with high membrane S1PR1 had a roughly 3 years shorter mean time to recurrence on tamoxifen and just over 8 years shorter disease-specific survival. It has been speculated that these differences in recurrence and survival could be due to E2 activation of SphK1 leading to the activation of the ERK1/2 pathways downstream of S1PR3 (Watson et al., 2010). Similar observations were made in another study (Ohotski et al., 2013).

Interestingly, S1P levels in breast cancer patients with lymph node metastasis that correlate with poor prognosis were significantly higher than those with negative lymph nodes, consistent with the notion that S1P plays an important role in angiogenesis, lymphangiogenesis, and metastasis (Tsuchida et al., 2016). Another interesting finding was that SphK1 levels determined by immunohistochemistry in deadlier TNBC tumors were lower, in contrast with some earlier studies. However, the S1P levels were higher, possibly suggesting the tumor microenvironment is responsible for the increase in S1P, not the tumor itself. This agreed with their observation of higher levels of S1P in patients with increased white blood cells, and suggested that since TNBCs are more immunogenic and immune cells express SphK1 and secrete S1P, they could increase S1P levels in the microenvironment (Tsuchida et al., 2016).

In sum, high levels of SphK1 expression and resulting high levels of S1P are most likely related to poorer prognosis for most patients. This could be due the ability of SphK1/S1P axis to promote cancer cell growth, proliferation, survival, and drug

resistance. Thus, decreasing SphK1 expression and activity and S1P production could represent a new approach to improve prognosis of breast cancer.

SPHINGOSINE KINASE 1 IN ANIMAL MODELS OF BREAST CANCER PROGRESSION AND METASTASIS

Most of the data on SphK1 and its relationship to breast cancer in humans have come from analysis of tumor samples combined with patient follow-up data. An increasing number of studies have used mouse models to examine the role of the SphK1/S1P axis in breast cancer progression. The first observation was that breast cancer cells stably overexpressing SphK1 formed more and larger tumors in mice than vector transfectants with higher microvessel density in their periphery (Nava et al., 2002). Similar results were obtained by orthotopically implanting 4T1-luc2 murine breast cancer cells into the mammary fat pads of immune competent female mice (Nagahashi et al., 2012). The 4T1-luc2 tumors are rapidly growing and metastasize first to the lymph nodes and then the lungs, reminiscent to human breast cancer progression. Interestingly, circulating levels of S1P in tumor bearing mice were also significantly increased. Treatment of these mice with the specific SphK1 inhibitor SKI-1 decreased plasma S1P levels concomitantly with significant reductions in tumor volume, weight, and mitotic activity as well as lymph node and lung metastsis (Nagahashi et al., 2012). Moreover, cancer stem cells overexpressing SphK1 had increased ability to develop tumors in nude mice. Tumorigenicity of these cancer stem cells was inhibited by S1PR3 knockdown or a S1PR3 antagonist indicating that S1P promotes expansion of cancer stem cells via S1PR3 by a ligand-independent Notch activation (Hirata et al., 2014).

Growth of tumors to beyond a certain size requires the formation of new blood vessels, termed angiogenesis, to continue to feed the rapidly growing and dividing cells (Nagahashi et al., 2012). To further spread throughout the body, the tumor cells usually extravasate and travel through the lymph system while also promoting formation of new lymph vessels through lymphangiogenesis. Both tumor size and metastasis are crucial in determining the staging and prognosis of a cancer (Nagahashi et al., 2016). There are also many cellular factors that contribute to angiogenesis and lymphangiogenesis, and perhaps others still to be discovered. However, it is becoming clear that S1P plays an important role in these processes. The angiogenic and lymphangiogenic actions of S1P are likely mediated via activation of S1PR1 on endothelial cells (Anelli et al., 2010; Nagahashi et al., 2012). As discussed above, S1P is commonly elevated in cancer tissues and in the circulation and also in lymph interstitial fluid from human breast cancer tumors (Nagahashi et al., 2016).

SPHK1/S1P/S1P RECEPTOR AXIS AS A THERAPEUTIC TARGET FOR BREAST CANCER

With such strong connections between SphK1/S1P/S1PR axis and the growth and progression of breast cancer cells, SphK1 and S1PR offer new and novel targets for possible future treatment avenues aimed at treating breast cancer, especially TNBC. Several preclinical studies have used mouse breast cancer models to investigate the effects of SphK1 inhibiters or S1PR modulators on tumor growth. A combination of the non-specific SphK inhibitor SKI-II with gefitinib, an EGFR inhibitor, significantly inhibited growth of xenograft MDA-MB-468 TNBC tumors whereas neither SKI-II or gefitinib alone had any effects (Martin et al., 2014). Another SphK1 inhibitor, SKI-5C, also

significantly reduced growth of tumors from another TNBC cell line, MDA-MB-231, in xenografted SCID mice (Datta et al., 2014). Using an improved syngeneic breast cancer cell implantation method that mimics human breast cancer biology better than conventional xenograft subcutaneous implantation, treatment with the specific SphK1 inhibitor SK1-I suppressed tumor growth of murine 4T1 breast cancer cells and S1P levels and reduced metastases to lymph nodes and lungs (Nagahashi et al., 2012).

Lastly, one of the most promising possible future avenues for breast cancer treatments that target the S1P axis is Fingolimod (FTY720), a sphingosine analog pro-drug currently used to treat multiple sclerosis that has long been known to have beneficial effects in many preclinical breast cancer models (Azuma et al., 2002; Deng et al., 2012; Hait et al., 2015; Rincon et al., 2015). FTY720 effects are not limited only to suppressing the development and progression of breast tumors on its own but also is an effective adjuvant therapy. Treatment with FTY720 potentiated the anti-cancer effects of doxorubicin in MDA-MB-231 xenograft tumors and particularly in MDA-MB-231 cells that acquired resistance to doxorubicin (Rincon et al., 2015). FTY720 has been shown to synergize with the effect of tumor necrosis factor-related apoptosis-inducing ligand (TRAIL) reducing tumor volume and inducing apoptosis in xenograft breast cancer models without affecting normal cells (Woo et al., 2015). FTY720 has several anti-cancer targets that contribute to its multi-potent effectiveness. When phosphorylated by SphK2, FTY720-P is a S1P mimetic that acts as a functional antagonist of S1PR1, reducing the persistent activation of STAT3 (Deng et al., 2012) and thus diminishes accumulation of regulatory T cells in tumors (Priceman et al., 2014).

We found that FTY720 is phosphorylated by nuclear SphK2 in breast cancer cells. FTY720-P accumulates in the nucleus and potently inhibits class I histone deacetylases (HDACs) leading to increased histone acetylations and expression of a restricted set of genes independently of its known effects on S1PRs. We also observed that feeding a high-fat diet accelerated formation of tumors and increased triple-negative spontaneous breast tumors in MMTV-PyMT transgenic mice and that oral treatment with FTY720 inhibited development and aggressiveness of spontaneous breast tumors in these mice, reduced HDAC activity and dramatically reversed high-fat diet-induced loss of ER and PR in advanced carcinoma. Like other HDAC inhibitors, treatment of ER-negative breast cancer cells with FTY720 reactivated expression of silenced ER and sensitized them to tamoxifen. Furthermore, treatment with FTY720 also re-expressed ER and increased therapeutic sensitivity of ER-negative syngeneic breast tumors to tamoxifen in vivo more strongly than a pan HDAC inhibitor.

Unphosphorylated FTY720 also has anti-cancer actions. It inhibits SphK1 by binding to an allosteric site that exerts auto-inhibition on the catalytic site. It also induces proteasomal degradation of SphK1 and thus inhibits actions of S1P (Lim et al., 2011). Moreover, part of the effectiveness of FTY720 in tumor suppression can be attributed to its ability to activate the tumor suppressor PP2A (Perrotti and Neviani, 2013; Saddoughi et al., 2013), which is commonly inhibited in breast cancer and is crucial for maintaining tumor cell properties (Rincon et al., 2015).

Overall these studies show that FTY720 is a multi-faceted drug with the potential to work as an effective anti-cancer drug by itself and also as an adjuvant to hormonal therapies, traditional chemotherapies, and even radiation therapies to treat not only ER-

positive tumors but also the more difficult TNBCs and tumors that develop resistance to chemotherapeutic agents. As FTY720 is already an FDA approved drug for treating humans, it is hoped that it can re-purposed for use as a cancer treatment.

Acknowledgements

This work was supported by grants from Department of Defense BCRP Program Award W81XWH-14-1-0086 and NIGMS grant R01GM043880 (S. Spiegel).

Competing interests statement

The authors declare no competing financial interests.

FIGURE LEGEND

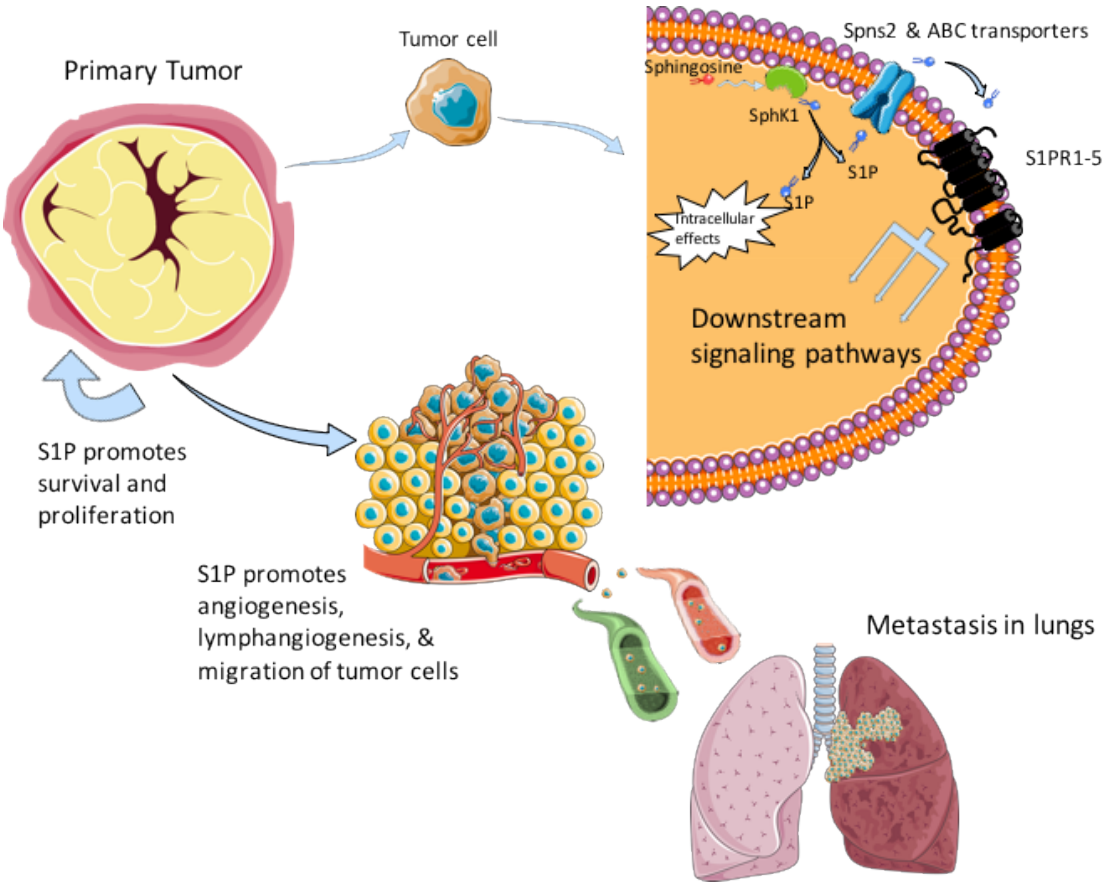

Figure 1. Role of the SphK1/S1P axis in breast tumor progression and metastasis.

REFERENCES

1. Alshaker, H., Krell, J., Frampton, A.E., Waxman, J., Blyuss, O., Zaikin, A., Winkler, M., Stebbing, J., Yague, E., Pchejetski, D., 2014. Leptin induces upregulation of sphingosine kinase 1 in oestrogen receptor-negative breast cancer via Src family kinase-mediated, janus kinase 2-independent pathway. Breast Cancer Res. Treat. 16(5), 426.
2. Alshaker, H., Wang, Q., Frampton, A.E., Krell, J., Waxman, J., Winkler, M., Stebbing, J., Cooper, C., Yague, E., Pchejetski, D., 2015. Sphingosine kinase 1 contributes to leptin-induced STAT3 phosphorylation through IL-6/gp130 transactivation in oestrogen receptor-negative breast cancer. Breast Cancer Res. Treat. 149(1), 59-67.
3. Anelli, V., Gault, C.R., Snider, A.J., Obeid, L.M., 2010. Role of sphingosine kinase-1 in paracrine/transcellular angiogenesis and lymphangiogenesis in vitro. FASEB J. 24(8), 2727-2738.
4. Azuma, H., Takahara, S., Ichimaru, N., Wang, J.D., Itoh, Y., Otsuki, Y., Morimoto, J., Fukui, R., Hoshiga, M., Ishihara, T., Nonomura, N., Suzuki, S., Okuyama, A., Katsuoka, Y., 2002. Marked prevention of tumor growth and metastasis by a novel immunosuppressive agent, FTY720, in mouse breast cancer models. Cancer Res. 62(5), 1410-1419.
5. Datta, A., Loo, S.Y., Huang, B., Wong, L., Tan, S.S., Tan, T.Z., Lee, S.C., Thiery, J.P., Lim, Y.C., Yong, W.P., Lam, Y., Kumar, A.P., Yap, C.T., 2014. SPHK1 regulates proliferation and survival responses in triple-negative breast cancer. Oncotarget 5(15), 5920-5933.

6. Deng, J., Liu, Y., Lee, H., Herrmann, A., Zhang, W., Zhang, C., Shen, S., Priceman, S.J., Kujawski, M., Pal, S.K., Raubitschek, A., Hoon, D.S., Forman, S., Figlin, R.A., Liu, J., Jove, R., Yu, H., 2012. S1PR1-STAT3 signaling is crucial for myeloid cell colonization at future metastatic sites. Cancer Cell 21(5), 642-654.
7. Gao, Y., Gao, F., Chen, K., Tian, M.L., Zhao, D.L., 2015. Sphingosine kinase 1 as an anticancer therapeutic target. Drug Des. Devel. Ther. 9, 3239-3245.
8. Hait, N.C., Allegood, J., Maceyka, M., Strub, G.M., Harikumar, K.B., Singh, S.K., Luo, C., Marmorstein, R., Kordula, T., Milstien, S., Spiegel, S., 2009. Regulation of histone acetylation in the nucleus by sphingosine-1-phosphate. Science 325(5945), 1254-1257.
9. Hait, N.C., Avni, D., Yamada, A., Nagahashi, M., Aoyagi, T., Aoki, H., Dumur, C.I., Zelenko, Z., Gallagher, E.J., Leroith, D., Milstien, S., Takabe, K., Spiegel, S., 2015. The phosphorylated prodrug FTY720 is a histone deacetylase inhibitor that reactivates ERalpha expression and enhances hormonal therapy for breast cancer. Oncogenesis 4, e156.
10. Hannun, Y.A., Obeid, L.M., 2008. Principles of bioactive lipid signalling: lessons from sphingolipids. Nat. Rev. Mol. Cell Biol. 9(2), 139-150.
11. Hirata, N., Yamada, S., Shoda, T., Kurihara, M., Sekino, Y., Kanda, Y., 2014. Sphingosine-1-phosphate promotes expansion of cancer stem cells via S1PR3 by a ligand-independent Notch activation. Nat. Commun. 5, 4806.
12. Igarashi, N., Okada, T., Hayashi, S., Fujita, T., Jahangeer, S., Nakamura, S.I., 2003. Sphingosine kinase 2 is a nuclear protein and inhibits DNA synthesis. J. Biol. Chem. 278(47), 46832–46839.

13. Kihara, Y., Maceyka, M., Spiegel, S., Chun, J., 2014. Lysophospholipid receptor nomenclature review: IUPHAR Review 8. Br. J. Pharmacol. 171(15), 3575-3594.
14. Klinge, C.M., 2001. Estrogen receptor interaction with estrogen response elements. Nucleic Acids Res. 29(14), 2905-2919.
15. Ko, P., Kim, D., You, E., Jung, J., Oh, S., Kim, J., Lee, K.H., Rhee, S., 2016. Extracellular Matrix Rigidity-dependent Sphingosine-1-phosphate Secretion Regulates Metastatic Cancer Cell Invasion and Adhesion. Sci. Rep. 6, 21564.
16. Kotelevets, N., Fabbro, D., Huwiler, A., Zangemeister-Wittke, U., 2012. Targeting sphingosine kinase 1 in carcinoma cells decreases proliferation and survival by compromising PKC activity and cytokinesis. PLoS One 7(6), e39209.
17. Lee, H., Deng, J., Kujawski, M., Yang, C., Liu, Y., Herrmann, A., Kortylewski, M., Horne, D., Somlo, G., Forman, S., Jove, R., Yu, H., 2010. STAT3-induced S1PR1 expression is crucial for persistent STAT3 activation in tumors. Nat. Med. 16(12), 1421-1428.
18. Liang, J., Nagahashi, M., Kim, E.Y., Harikumar, K.B., Yamada, A., Huang, W.C., Hait, N.C., Allegood, J.C., Price, M.M., Avni, D., Takabe, K., Kordula, T., Milstien, S., Spiegel, S., 2013. Sphingosine-1-phosphate links persistent STAT3 activation, chronic intestinal inflammation, and development of colitis-associated cancer. Cancer Cell 23(1), 107-120.
19. Lim, K.G., Tonelli, F., Li, Z., Lu, X., Bittman, R., Pyne, S., Pyne, N.J., 2011. FTY720 analogues as sphingosine kinase 1 inhibitors: enzyme inhibition kinetics, allosterism, proteasomal degradation, and actin rearrangment in MCF-7 breast cancer cells J. Biol. Chem. 286(21), 18633-18640.

20. Maceyka, M., Harikumar, K.B., Milstien, S., Spiegel, S., 2012. Sphingosine-1-phosphate signaling and its role in disease. Trends Cell Biol. 22(1), 50-60.
21. Maceyka, M., Spiegel, S., 2014. Sphingolipid metabolites in inflammatory disease. Nature 510(7503), 58-67.
22. Maczis, M., Milstien, S., Spiegel, S., 2016. Sphingosine-1-phosphate and estrogen signaling in breast cancer. Adv. Biol. Regul. 60, 160-165.
23. Maiti, A., Takabe, K., Hait, N.C., 2017. Metastatic triple-negative breast cancer is dependent on SphKs/S1P signaling for growth and survival. Cell Signal. 32, 85-92.
24. Martin, J.L., de Silva, H.C., Lin, M.Z., Scott, C.D., Baxter, R.C., 2014. Inhibition of insulin-like growth factor-binding protein-3 signaling through sphingosine kinase-1 sensitizes triple-negative breast cancer cells to EGF receptor blockade. Mol. Cancer Ther. 13(2), 3163-3128.
25. Nagahashi, M., Ramachandran, S., Kim, E.Y., Allegood, J.C., Rashid, O.M., Yamada, A., Zhao, R., Milstien, S., Zhou, H., Spiegel, S., Takabe, K., 2012. Sphingosine-1-phosphate produced by sphingosine kinase 1 promotes breast cancer progression by stimulating angiogenesis and lymphangiogenesis. Cancer Res. 72(3), 726-735.
26. Nagahashi, M., Yamada, A., Miyazaki, H., Allegood, J.C., Tsuchida, J., Aoyagi, T., Huang, W.C., Terracina, K.P., Adams, B.J., Rashid, O.M., Milstien, S., Wakai, T., Spiegel, S., Takabe, K., 2016. Interstitial Fluid Sphingosine-1-Phosphate in Murine Mammary Gland and Cancer and Human Breast Tissue and Cancer Determined by Novel Methods. J. Mammary Gland Biol. Neoplasia 21(1-2), 9-17.

27. Nava, V.E., Hobson, J.P., Murthy, S., Milstien, S., Spiegel, S., 2002. Sphingosine kinase type 1 promotes estrogen-dependent tumorigenesis of breast cancer MCF-7 cells. Exp. Cell Res. 281(1), 115-127.
28. Newton, J., Lima, S., Maceyka, M., Spiegel, S., 2015. Revisiting the sphingolipid rheostat: Evolving concepts in cancer therapy. Exp. Cell Res. 333(2), 195-200.
29. Ohotski, J., Edwards, J., Elsberger, B., Watson, C., Orange, C., Mallon, E., Pyne, S., Pyne, N.J., 2013. Identification of novel functional and spatial associations between sphingosine kinase 1, sphingosine 1-phosphate receptors and other signaling proteins that affect prognostic outcome in estrogen receptor-positive breast cancer. Int. J .Cancer 132(3), 605-616.
30. Perrotti, D., Neviani, P., 2013. Protein phosphatase 2A: a target for anticancer therapy. Lancet Oncol. 14(6), e229-238.
31. Pinho, F.G., Frampton, A.E., Nunes, J., Krell, J., Alshaker, H., Jacob, J., Pellegrino, L., Roca-Alonso, L., de Giorgio, A., Harding, V., Waxman, J., Stebbing, J., Pchejetski, D., Castellano, L., 2013. Downregulation of microRNA-515-5p by the estrogen receptor modulates sphingosine kinase 1 and breast cancer cell proliferation. Cancer Res. 73(19), 5936-5948.
32. Pitson, S.M., Moretti, P.A., Zebol, J.R., Lynn, H.E., Xia, P., Vadas, M.A., Wattenberg, B.W., 2003. Activation of sphingosine kinase 1 by ERK1/2-mediated phosphorylation. EMBO J. 22(20), 5491-5500.
33. Priceman, S.J., Shen, S., Wang, L., Deng, J., Yue, C., Kujawski, M., Yu, H., 2014. S1PR1 is crucial for accumulation of regulatory T cells in tumors via STAT3. Cell Rep. 6(6), 992-999.

34. Pyne, N.J., Pyne, S., 2010. Sphingosine 1-phosphate and cancer. Nat. Rev. Cancer 10(7), 489-503.

35. Rincon, R., Cristobal, I., Zazo, S., Arpi, O., Menendez, S., Manso, R., Lluch, A., Eroles, P., Rovira, A., Albanell, J., Garcia-Foncillas, J., Madoz-Gurpide, J., Rojo, F., 2015. PP2A inhibition determines poor outcome and doxorubicin resistance in early breast cancer and its activation shows promising therapeutic effects. Oncotarget 6(6), 4299-4314.

36. Ruckhaberle, E., Rody, A., Engels, K., Gaetje, R., von Minckwitz, G., Schiffmann, S., Grosch, S., Geisslinger, G., Holtrich, U., Karn, T., Kaufmann, M., 2008. Microarray analysis of altered sphingolipid metabolism reveals prognostic significance of sphingosine kinase 1 in breast cancer. Breast Cancer Res. Treat. 112(1), 41-52.

37. Saddoughi, S.A., Gencer, S., Peterson, Y.K., Ward, K.E., Mukhopadhyay, A., Oaks, J., Bielawski, J., Szulc, Z.M., Thomas, R.J., Selvam, S.P., Senkal, C.E., Garrett-Mayer, E., De Palma, R.M., Fedarovich, D., Liu, A., Habib, A.A., Stahelin, R.V., Perrotti, D., Ogretmen, B., 2013. Sphingosine analogue drug FTY720 targets I2PP2A/SET and mediates lung tumour suppression via activation of PP2A-RIPK1-dependent necroptosis. EMBO Mol. Med. 5(1), 105-121.

38. Sankala, H.M., Hait, N.C., Paugh, S.W., Shida, D., Lepine, S., Elmore, L.W., Dent, P., Milstien, S., Spiegel, S., 2007. Involvement of sphingosine kinase 2 in p53-independent induction of p21 by the chemotherapeutic drug doxorubicin. Cancer Res. 67(21), 10466-10474.

39. Sarkar, S., Maceyka, M., Hait, N.C., Paugh, S.W., Sankala, H., Milstien, S., Spiegel, S., 2005. Sphingosine kinase 1 is required for migration, proliferation and survival of MCF-7 human breast cancer cells. FEBS Lett. 579(24), 5313-5317.
40. Sukocheva, O., Wadham, C., 2014. Role of sphingolipids in oestrogen signalling in breast cancer cells: an update. J. Endocrinol. 220(3), R25-R35.
41. Sukocheva, O., Wadham, C., Holmes, A., Albanese, N., Verrier, E., Feng, F., Bernal, A., Derian, C.K., Ullrich, A., Vadas, M.A., Xia, P., 2006. Estrogen transactivates EGFR via the sphingosine 1-phosphate receptor Edg-3: the role of sphingosine kinase-1. J. Cell Biol. 173(2), 301-310.
42. Sukocheva, O., Wadham, C., Xia, P., 2013. Estrogen defines the dynamics and destination of transactivated EGF receptor in breast cancer cells: role of S1P(3) receptor and Cdc42. Exp. Cell Res. 319(4), 455-465.
43. Takabe, K., Kim, R.H., Allegood, J.C., Mitra, P., Ramachandran, S., Nagahashi, M., Harikumar, K.B., Hait, N.C., Milstien, S., Spiegel, S., 2010. Estradiol induces export of sphingosine 1-phosphate from breast cancer cells via ABCC1 and ABCG2. J. Biol. Chem. 285(14), 10477-10486.
44. Takabe, K., Paugh, S.W., Milstien, S., Spiegel, S., 2008. "Inside-out" signaling of sphingosine-1-phosphate: therapeutic targets. Pharmacol. Rev. 60(2), 181-195.
45. Tsuchida, J., Nagahashi, M., Nakajima, M., Moro, K., Tatsuda, K., Ramanathan, R., Takabe, K., Wakai, T., 2016. Breast cancer sphingosine-1-phosphate is associated with phospho-sphingosine kinase 1 and lymphatic metastasis. J. Surg. Res. 205(1), 85-94.

The authors have no conflicts of interest to declare.
Please note that this is an invited review for a special issue edited by Prof. Lucio Cocco for the Special issue, volume 67 Advances in Biological Regulation.
Bologna October 2-3, 2017

Sarah Spiegel
Kurt Geffken